ADVANCED ION SOURCE

Harry J. King

Hughes Research Laboratories

Prepared for:

Air Force Technical Applications Center
Advanced Research Projects Agency

21 March 1973

ADVANCED ION SOURCE

15

PHASE I REPORT
PROJECT SCIENTIST: H. KING
213-456-6411

Sponsored by
ADVANCED RESEARCH PROJECTS AGENCY
ARPA ORDER NO. 1702, AMD. 3

AFTAC PROJECT AUTHORIZATION NO. VT/3423/-/ETR
PROGRAM CODE NO. 3F10
CONTRACT NO. F08606-73-C-0038
EFFECTIVE: 21 MARCH 1973
EXPIRATION: 20 DECEMBER 1974
AMOUNT: $219,780.00

PROJECT OFFICER: CAPT. JOHN P. OSS
HQ USAF (AFTAC/TRE)
PATRICK AIR FORCE BASE, FLORIDA 32925
305-494-2822

DISTRIBUTION UNLIMITED

This research was supported by the Advanced Research Projects Agency of the Department of Defense, and was monitored by HQ USAF (AFTAC/TD-4C), Patrick Air Force Base, Florida 32925 under Contract No. F08606-73-C-0038.

HUGHES

HUGHES AIRCRAFT COMPANY
RESEARCH LABORATORIES

ADVANCED ION SOURCE

Phase I Report

Project Scientist: H. King
213-456-6411

Sponsored by
Advanced Research Projects Agency
ARPA Order No. 1702, Amd 3

AFTAC Project Authorization No. VT/3423/-/ETR
Program Code No. 3F10
Contract No. F08606-73-C-0038
Effective: 21 March 1973
Expiration: 20 December 1974
Amount: $219,780.00

Project Officer: Capt. John P. Oss
HQ USAF (AFTAC/TRE)
Patrick Air Force Base, Florida 32925
305-494-2822

This research was supported by the Advanced Research Projects Agency of the Department of Defense, and was monitored by HQ USAF (AFTAC/TD-4C), Patrick Air Force Base, Florida 32925 under Contract No. F08606-73-C-0038.

TABLE OF CONTENTS

I.	INTRODUCTION.	1
II.	PROGRAM OUTLINE	3
III.	ADVANCED ION SOURCE DESIGN.	5
	A. Cesium Ion Source	5
	B. Iodine Source	18
	C. Prototype System Design	39
IV.	CONCLUSIONS AND SUMMARY	53
	REFERENCES.	55
	DD Form 1473	

UNCLASSIFIED

Security Classification

DOCUMENT CONTROL DATA - R&D AD772833

(Security classification of title, body of abstract and indexing annotation must be entered when the overall report is classified)

1. ORIGINATING ACTIVITY *(Corporate author)*
Hughes Research Laboratories
3011 Malibu Canyon Road
Malibu, California 90265

2a. REPORT SECURITY CLASSIFICATION
Unclassified

2b. GROUP

3. REPORT TITLE

ADVANCED ION SOURCE (Phase I Report)

4. DESCRIPTIVE NOTES *(Type of report and inclusive dates)*
Phase I, Final Report 21 March 73 – 21 June 73

5. AUTHOR(S) *(First name, middle initial, last name)*

Harry J. King

6. REPORT DATE	7a. TOTAL NO. OF PAGES	7b. NO. OF REFS
21 March 1973	55 58	6

8a. CONTRACT OR GRANT NO.	9a. ORIGINATOR'S REPORT NUMBER(S)
F08606-73-C-0038	Phase I
b. PROJECT, TASK, WORK UNIT NOS. 3F10	
c. DOD ELEMENT	9b. OTHER REPORT NO(S) *(Any other numbers that may be assigned this report)*
d. DOD SUBELEMENT	----

10. DISTRIBUTION STATEMENT

Distribution unlimited.

11. SUPPLEMENTARY NOTES	12. SPONSORING MILITARY ACTIVITY
N/A	Advanced Research Projects Agency

13. ABSTRACT

The analytic and experimental studies conducted during Phase I of this program indicate that it is possible to design both cesium and iodine sources to meet the specified brightness requirements of 200 and 100 A/cm^2 sr respectively. No reasons were uncovered as to why these two types of sources cannot operate in the same vacuum environment in such a manner that the ion species available to the AMS can be rapidly changed. Prototype hardware will be developed in Phase II to demonstrate this ability.

DD FORM 1 NOV 65 1473

UNCLASSIFIED

Security Classification

14. KEY WORDS	LINK A		LINK B		LINK C	
	ROLE	WT	ROLE	WT	ROLE	WT
Cesium ion beam						
Iodine ion beam						
Positive ions						
Negative ions						
Contact ionization						
Ion optics						
Ion beam brightness						

LIST OF ILLUSTRATIONS

Figure		Page
1	Rate of cesium atom and ion evaporization from a tungsten surface versus the adatom surface coverage for three surface temperatures.	7
2	Cesium-ion current density at the critical point versus the corresponding critical temperature, for tungsten. . . .	8
3	Electron emission from a copper surface onto which cesium vapor is flowing with an arrival rate (atoms/cm^2 sec) shown as the parameter on the curves.	11
4	Maximum brightness may be achieved by generating a beam somewhat larger than required and aperturing so as to use only the central portion.	13
5	Computer generated trajectories for Pierce extraction geometry with full space charge and curved cathode	14
6	Computer generated trajectories for Pierce extraction geometry with full space charge and flat cathode	14
7	Computer generated trajectories for Pierce extraction geometry with half space charge and flat cathode	14
8	Calculated perveance line for Pierce extraction geometry shown in Fig. 6	15
9	Calculated beam envelope containing 95% of the extracted current as a function of distance from the cathode for two transverse ion temperatures	17
10	Calculated current density as a function of radius for cathode temperture of 0.32 eV and 0.325 mm cathode diameter at the crossover	19
11	Cutaway view of the high field-point geometry ion/electron source.	22

Figure		Page
12	Enlarged cross-sectional view of the cathode-grid-anode region.	24
13	Cross sectional view of the test chamber showing the separation of the electrons from the negative ions	26
14	Schematic of circuit used in tests	26
15	Plot of electron to ion current ratios as a function of cathode termperature.	29
16	Equivalent electron current and perveance as a function of effective cathode diameter for different electron to iodine current ratios f	31
17	Schematic and typical characteristics of short-focus hairpin filament gun.	34
18	Schematic and typical operating characteristics of tele-focus type gun	35
19	Computer trajectory calculations for HRL point cathode gun design for two cathode positions.	37
20	Graph showing decrease in effective I- brightness as a functior of electron to ion ratio f for different point cathode type geometries.	38
21	Layout of cesium ion source.	40
22	Plasma sprayed cathode heater.	42
23	Electrical schematic of cesium ion source. . .	43
24	Schematic of iodine source	44
25	Electrical schematic of negative iodine source	46
26	Detail of rotating assembly used to reposition cesium or iodine sources.	47
27	Isometric view of source chamber showing detail of source positioning mechanism	48
28	Layout of ion source vacuum chamber.	50

I. INTRODUCTION

The Advanced Ion Source (AIS) with which the report deals will be a major subsystem of the Advance Mass Separator (AMS)[1] currently under development by AFTAC. This AMS will serve as an exceedingly high resolution analyzer to determine the composition of surface layers or small particles. It accomplishes this analysis by mass analyzing the ions which are sputtered from the sample surface by a highly focussed ion beam. It has been demonstrated that incident ions of both electropositive and electronegative species (here Cs^+ and I^-) are required to provide adequate sensitivity over the whole periodic table. Clearly, the more intense the incident ion beam the faster the analysis may be accomplished. Therefore, the goal of the present project (i.e., to provide a bright, stable source of Cs^+ and I^-) directly affects the speed and resolution of the instrument.

II. PROGRAM OUTLINE

The program to develop the AIS has been divided into four phases:

Phase I – Design Study

Phase II – Prototype Hardware Development

Phase III – Deliverable Hardware Fabrication and Verification

Phase IV – Integration at AMS Facility.

This report is a summary of the Phase I results. It has been divided into three main sections. The first section deals with the design of the cesium source which was based primarily on previous well documented results obtained in the Hughes Research Laboratories (HRL) Ion Propulsion program. The second section deals with the design of the negative iodine source and the experiments that were conducted to verify the basic design parameters. The final section illustrates how these sources will be packaged to provide a functional system which interfaces properly with the AMS.

III. ADVANCED ION SOURCE DESIGN

A. Cesium Ion Source

The cesium ion source to be designed for this application is very similar to the small cesium contact ion thrusters which have been constructed at HRL for several years. This technology has been described in great detail by G.R. Brewer of our laboratory in his book Ion Propulsion[2] to which the readers referred for detailed discussions and an extensive bibliography.

1. The Porous Tungsten Ionizer

a. Contact Ionization — The cesium atom has a relatively low work function (or electron affinity) and will, therefore, give up an electron to a high work function surface from which it is evaporated. In particular, if cesium vapor is passed through a hot porous tungsten plug, it is possible to extract a fully ionized beam of positive cesium ions from the downstream surface. This basic process is described by the Saha Equation

$$\eta_i = \frac{V_i}{u} = \frac{1}{1 + 2\exp\left(\frac{I - \phi}{kT_i}\right)} \qquad (1)$$

where

V_i = evaporation rate of ions
u = cesium arrival rate
η_i = ionization efficiency
T_i = ionizer temperature
I = ionization potential
ϕ = surface work function

For cesium on tungsten $\phi - I = 4.55 - 3.89 = 0.66$ eV.

As the surface coverage of cesium goes up, the surface work function is lowered and the ionization efficiency is reduced, as shown in Fig. 1. From this figure it can be seen that it is important to maintain the arrival rate and emitter temperature such that the cesium surface coverage is approximately 2%. This cesium-tungsten system exhibits an interesting behavior as a function of surface temperature. If the cesium atom arrival rate on the surface is constant (as indicated by the horizontal line μ_a in Fig. 1) and the surface temperature is gradually raised from 1300°K (at which the surface coverage will be approximately 20%), it is seen that the atom evaporation rate will increase and the surface coverage will decrease (in such a way that the total evaporation rate is always equal to the arrival rate) until point B is reached. If the temperature is increased further the evaporation rate is increased above the arrival rate and the surface coverage will decrease again until a stable point A is reached. This last change in surface coverage will occur with a very small change in temperature. At this temperature the evaporation suddenly changes from one in which atoms predominate to one which consists mostly of ion emission; this temperature is called the critical temperature. Since operation along the left branch of this curve is always desirable, it is essential that the ionizer always be operated above this critical temperature value.

In a practical situation this phenomena manifests itself as shown in Fig. 2, which illustrates the abrupt increase in ion current observed when the critical temperature is reached. Note that the critical temperature point is a function of both the cesium arrival rate and the cleanliness or oxidation state of the tungsten surface. It is clear that the critical temperature sets a lower temperature limit for the ionizer operation.

b. Porous Tungsten Ionizers — The above criteria apply rigorously to only a smooth, uniformly coated ionizing surface. In practice this geometry is very difficult to effectively use and the ionzer actually consists of a porous tungsten pellet through which cesium vapor is passed. Since there is a net flow of cesium from the

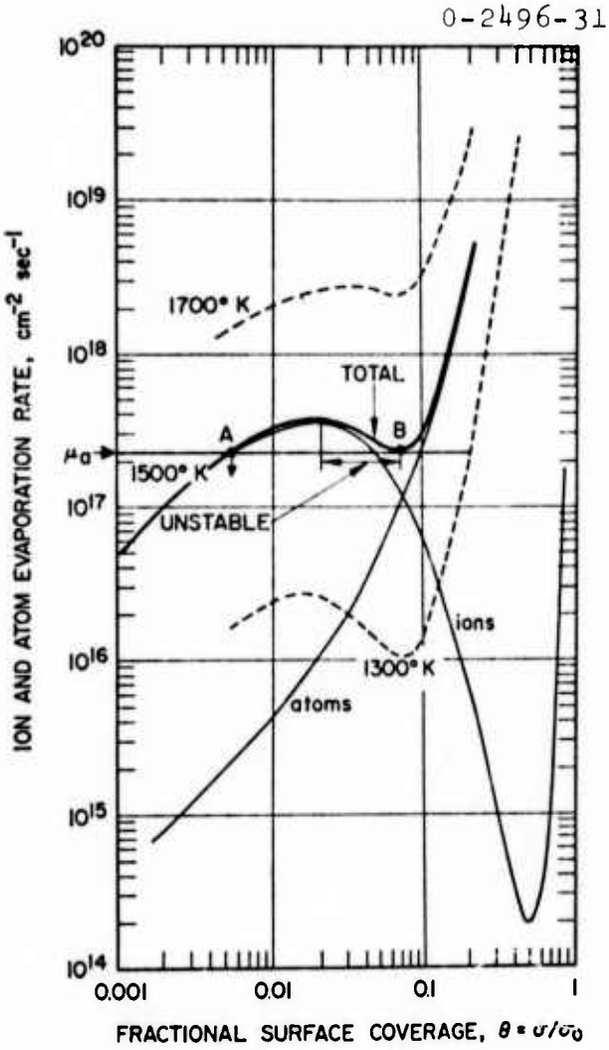

Fig. 1.
Rate of cesium atom and ion evaporation from a tungsten surface versus the adatom surface coverage for three surface temperatures. The heavy line shows the total (ion + atom) evaporation rate for 1500°K, σ = adsorbed cesium particles/cm^2; σ_o = monolayer surface density of cesium atoms on tungsten (3.56 x 10^{14}/cm^2).

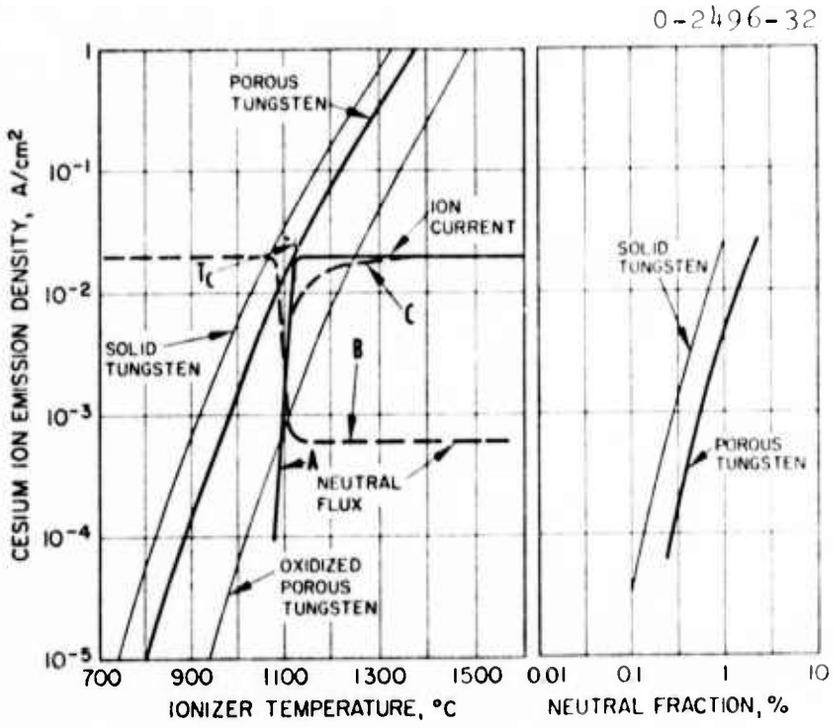

Fig. 2.
Cesium-ion current density at the critical point versus the corresponding critical temperature, for tungsten. Behavior of the ion current and neutral flux (curves A and B respectively) is shown as a function of temperature for one value of cesium arrival rate at the ionizing surface. The dashed curve portion (C) of the ion current curve shows the effect of a carbon contaminant. The curves at the right show the corresponding increase in neutral cesium efflux as current density is increased.

pores, there will be a range of surface coverage and local variations in ion current density over the ionizer surface. As shown in Fig. 2, this makes both the critical temperature and the average neutral efflux for porous tungsten somewhat higher than the theoretical value for smooth tungsten.

The ionizer performance can be improved by increasing the number and uniformity of distribution of the pores in the ionizer. Modern ionizer materials are sintered from spherical tungsten powder which has been carefully sorted into fractions of very narrow particle size. A good ionizer material for this application is one fabricated from powder ~4.0 μm in diameter which has been pressed and sintered to a density of 80% to produce approximately 3×10^6 pores/cm^2, each approximately 2 μm in diameter.

Smaller pores can in principle be made; however, they tend to gradually sinter closed at the ionizer operating temperature. This sirtering process gradually occurs for all ionizer materials and densities. Typically, lifetimes of 10^4 hours may be anticipated for carefully selected ionizer materials.

This sintering process sets an upper limit to the ionizer operating temperature and implies that the nominal temperature should be just adequate to assure that the critical temperature for the particular surface condition and cesium flowrate is exceeded at all points on the ionizer.

The small pores and finite thickness of the porous ionizer create a relatively high flow impedance for the cesium vapor. Typically, only one atom in 10^5 which impinge on the upstream side of the ionizer actually penetrate to the ionizing side. Cesium vapor pressure behind the ionizer must, therefore, be of the order of 10 Torr.

2. The Accelerator Electrode

The accelerator electrode is situated immediately downstream of the ionizer. It produces the field gradient necessary to extract and focus the cesium ions emitted from the ionizer surface. Care must be exercised in the choice of both the base material and the operating temperature to assure continued stable source operation.

a. Backsputtered Atoms – Even though the ion gun structure may be very carefully designed, some high velocity ions will strike the accelerator and sputter material from the accelerator onto the ionizer. If this material builds up on the ionizing surface, it will modify the surface work function, clog the pores and generally degrade ionizer performance. The most practical solution to this problem is to make the accelerator from copper which has a sufficiently high vapor pressure that it evaporates from the ionizer rapidly enough that a monolayer does not form. For this same reason it is imperative that all downstream apertures and probes, which may be in the beam for any appreciable time, should also be made of copper to prevent ionizer degradation.

b. Electron Emission – Since the accelerator is held at a high negative potential and is covered with cesium (which has a low work function), it is able to emit copious quantities of electrons if its temperature is not controlled. This will be indistinguishable in the control circuitry from positive ion current and will, therefore, decrease stability and may saturate the high voltage power supply. The electron emission from cesiated copper is shown in Fig. 3, for various cesium arrival rates. From this figure, it may be seen that electron emission should not be a problem if the accelerator surface is maintained below $\sim 300^{\circ}C$. While this is difficult for some of the larger thrusters, it is quite practical for the small ionizer to be used here.

Electron emission from the accelerator is considerably enhanced if the surfaces are not smooth or if "whiskers" of metal are permitted to grow on the surface. These effects can be reduced by careful assembly procedures, a clean, oxygen-free operating environment, and a controlled conditioning period when high voltage is first applied to a new structure.

3. Cesium Ion Extraction System

As anticipated in our proposal, a convergent Pierce gun is proving to be a highly suitable extraction system configuration for cesium ions in the advanced ion source. In order to provide a

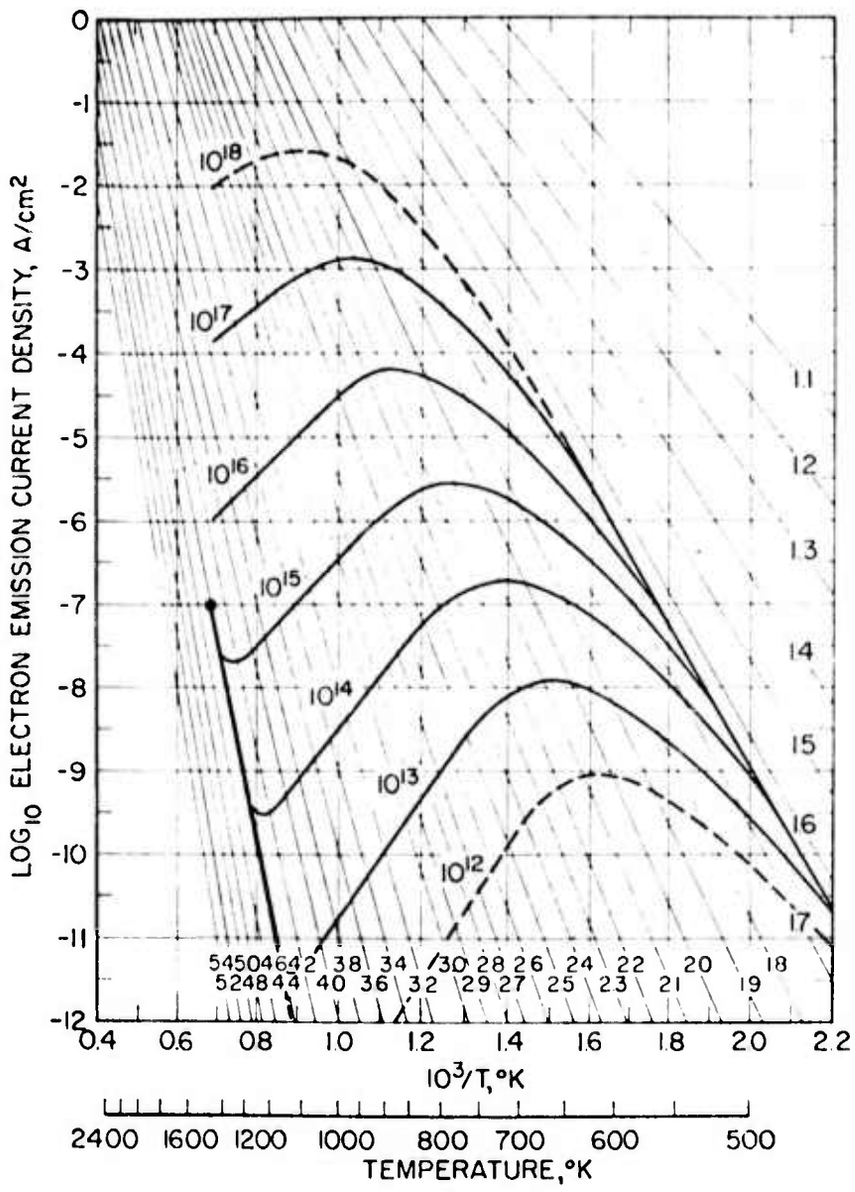

Fig. 3.
Electron emission from a copper surface onto which cesium vapor is flowing with an arrival rate (atoms/cm^2 sec) shown as the parameter on the curves. The abscissa is temperature of the copper substrate. The numbers on the light diagonal lines refer to values of work function in electron volts.

beam brightness at the virtual object ($B_o = J_A/\pi\,\alpha^2$) that approaches the maximum theoretical brightness of the ion source ($B_{th} = J_{se}V_o/\pi kT$), an ion beam will be generated for which the crossover diameter is considerably greater than 100 μm. Since the radial current density distribution is gaussian at the crossover, only the very central (paraxial) region of the beam has maximum current density and hence maximum brightness, as shown in Fig. 4. Here a nominal beam diameter of 1 mm is shown apertured down to 0.1-mm diameter at the crossover. Our efforts thus far have been to design an electrode geometry which produces this type of crossover, taking into account the effects of space charge and transverse ion velocities. The actual placement of limiting apertures which define the 100-μm diameter virtual object in the advanced ion column has yet to be determined. Ion trajectories for three spacecharge-extraction system configurations were computed and are shown in Figs. 5, 6, and 7. These trajectories assume that the ions leave normal to the emitter surface (i.e., with zero transverse velocity). The cases in Figs. 5 and 6 correspond to spacecharge limited currents extracted from ionizers that are slightly concave (radius of curvature = 24 R_{cath}) and flat respectively. The total extracted currents for these cases is the same (~57 μA of Cs as 20 kV). The main difference is that the ion trajectories for the flat ionizer case are more parallel. The operation of these extraction systems in the spacecharge limited mode produces an extracted current that is proportional to the extraction voltage to the 3/2 power. The proportionality constant or perveance is only a function of the electrode geometry. Thus, these extraction systems would provide beams with identical trajectories if operated anywhere on the line in Fig. 8. The actual ion source can be operated in a flow limited mode, however, by limiting the cesium flow. This is desirable to achieve optimum control. The flow limited mode corresponds, for example, to point P in Fig. 8, in which case the cesium flow rate is limiting the extracted current to half of its spacecharge limited value. Under this condition the ion trajectories of the extracted beam can vary considerably from their spacecharge limited counterparts. Our computer program for the flat ionizer geometry of Fig. 6 was rerun with the current fixed at half

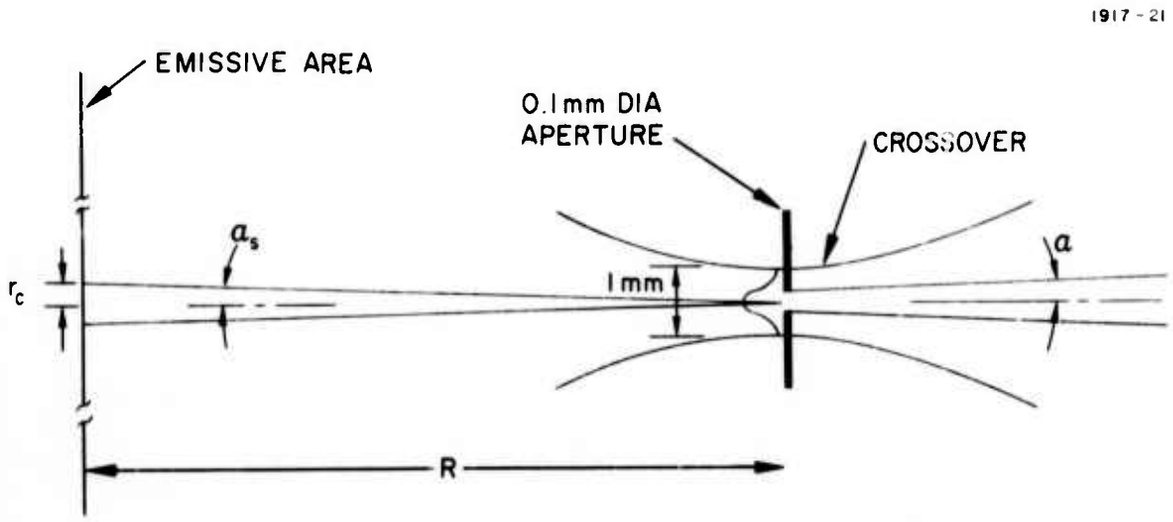

Fig. 4. Maximum brightness may be achieved by generating a beam somewhat larger than required and aperturing so as to use only the central portion.

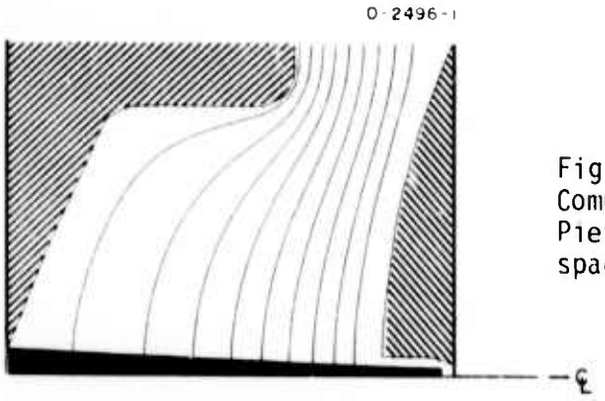

Fig. 5.
Computer generated trajectories for Pierce extraction geometry with full space charge and curved cathode.

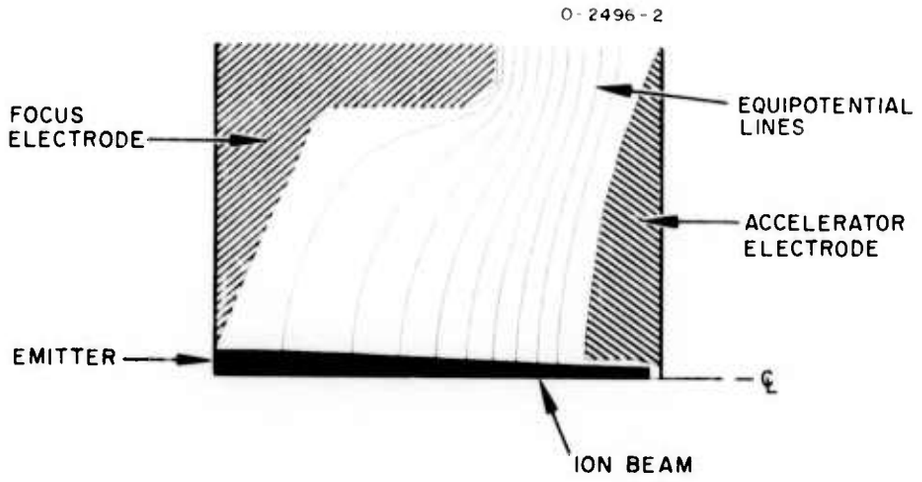

Fig. 6.
Computer generated trajectories for Pierce extraction geometry with full space charge and flat cathode. (Note that the beam waist is larger and the convergent angle smaller than for the curved cathode shown in Fig. 5.)

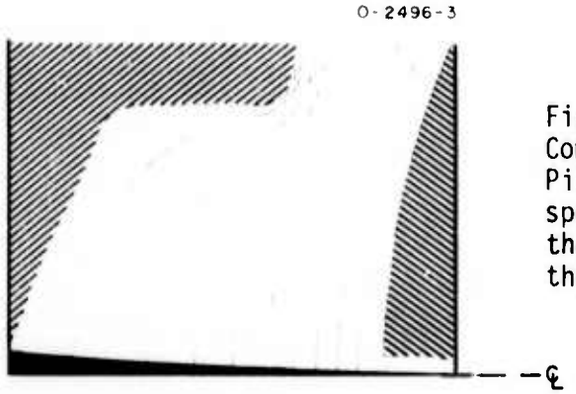

Fig. 7.
Computer generated trajectories for Pierce extraction geometry with half space charge and flat cathode. (Note that the beam is much more convergent than that of Fig. 6.)

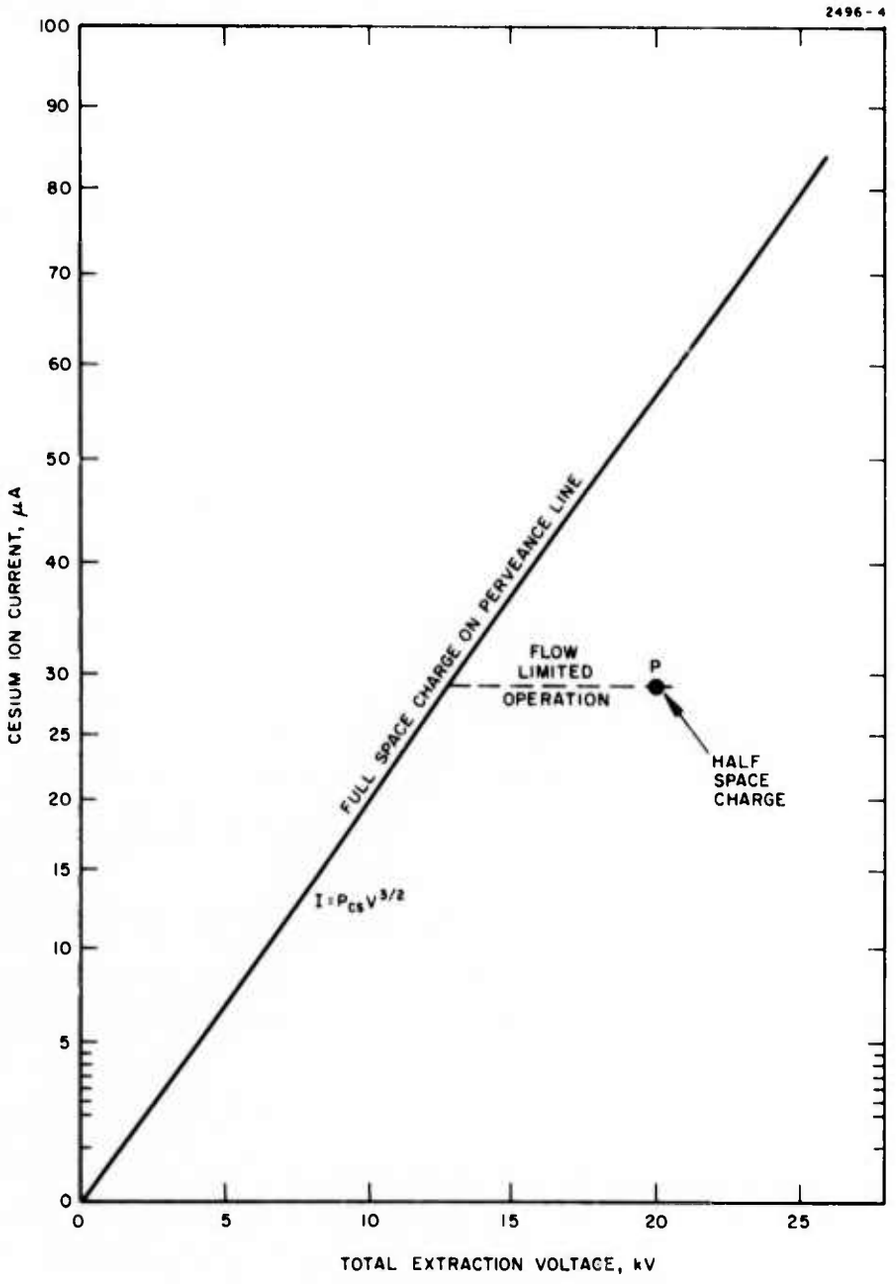

Fig. 8. Calculated perveance line for Pierce extraction geometry shown in Fig. 6. $P_{Cs} = 2.02 \times 10^{-11}$ A/V$^{3/2}$ Point P shows operation at a higher voltage than required. See trajectories calculated in Fig. 7.

its original value. The new trajectories, shown in Fig. 7, are clearly more convergent than in the full current case (Fig. 6).

In view of the long throw (~28 cm) from the virtual object to the first lens in the advanced ion column, it appears that the extraction system design should produce the most parallel beam possible. (The acceptance half-angle is ~3.5 mrad). We, therefore, choose the extraction system configuration of Fig. 6, and require that it be operated in the spacecharge limited mode.

The ion trajectories calculated above without the effects of initial transverse velocities give qualitatively correct beam trajectories (e.g., the angles are representative). But other beam properties, such as the location and current density profile at the crossover must be calculated in the presence of transverse velocity effects. Our second computer program was used to compute the envelopes of 95% of the extracted current from the geometry of Fig. 6. The results are shown in Fig. 9 for transverse ion velocities corresponding to temperatures of 1400°K (a lower bound) and 5800°K (a reasonable upper bound). The crossover locations in both cases are downstream of the extraction electrode (i.e., external crossovers).

The actual length scale in our extraction system is the only remaining parameter that is unspecified. The designs have the property that all the dimensions, including the trajectories, can be multiplied by a constant factor without affecting the extracted current (e.g., 57 μA of cesium at 20 kV). The two constraints on choosing the scale are set by the current density at the source and voltage breakdown at the highest field point of the electrode geometry. The current densities at the source and crossover increase with reduced geometry; hence, this is the direction to go for high brightness. Table I presents three cases of scaling which produce sufficient current density to obtain the desired brightness of 200 A/cm^2 sr for transverse ion energies of 0.23 eV, 0.32 eV, and 0.5 eV. The middle case of 0.32 eV requires a source current density of 10 mA/cm^2 which is reasonable for ionizer operation. The scaling for this case has the ionizer diameter equal to 0.085 in. The maximum electric field is ~90 kV/cm.

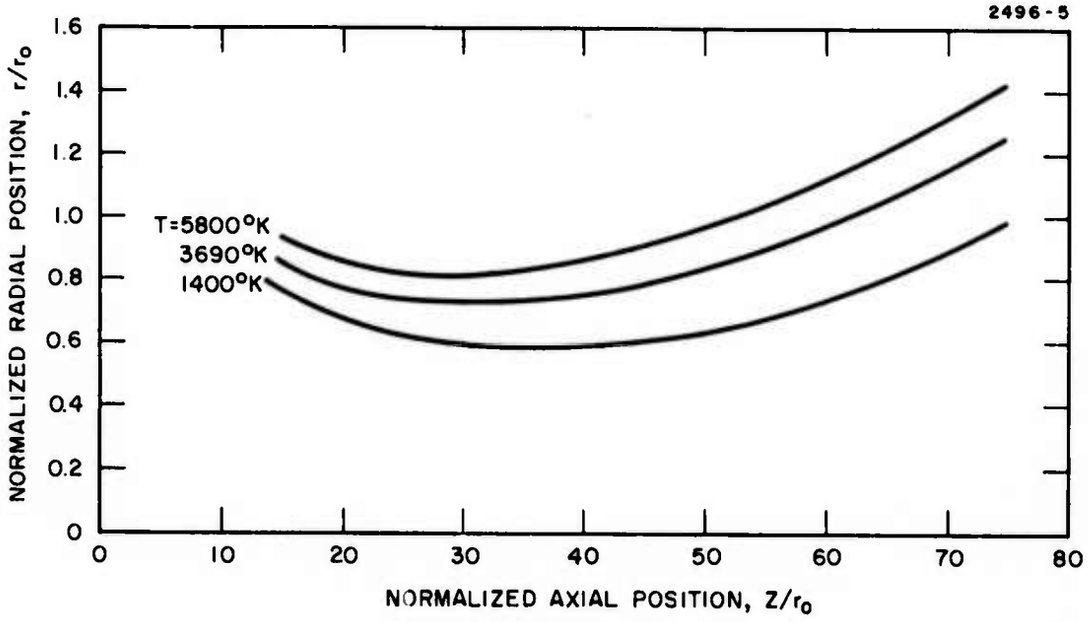

Fig. 9. Calculated beam envelope containing 95% of the extracted current as a function of distance from the cathode for two transverse ion temperatures. The greater random energy associated with the higher temperature has expanded the beam diameter.

TABLE I

Scaling Parameters and Maximum Field Gradients for Pierce Extraction Geometry of Fig. 6 for Different Ion Temperatures

V_o = 20 kV, B = 200 A/cm^2 sr, I_{cs} = 57 μA				
Design	ΔV_T, eV	J_{cath}, mA/cm^2	d_{cath}, cm	E_{max}, kV/cm
1	0.231	7.26	0.10	71.6
2	0.318	10.0	0.085	86.8
3	0.50	15.7	0.068	107.0

T958

The current density profile at the crossover for this case (J_s = 10 mA/cm^2, ΔV = 0.32 eV) is shown in Fig. 10. The current density in the 100 μm diameter central beam region is ~8 mA/cm^2 which is ~80% of the source current density. The nominal beam angle at the crossover is 3.6 mrad which yields a predicated beam brightness of ~200 A/cm^2 sr.

B. Iodine Source

1. Creation of Negative Iodine Ions

It is evident from the basic Saha Equation, used to define the creation of positive cesium ions on a tungsten surface, that it should also be possible to generate negative iodine ions on a low work function surface such as lanthanum hexaboride. While this process looked ideal from an analytical standpoint (for the production of the ion beam desired for this application) there is little experimental data to indicate the feasibility. The apparent reasons for this are the limited uses to which negative ions may be put plus the copious quantities of

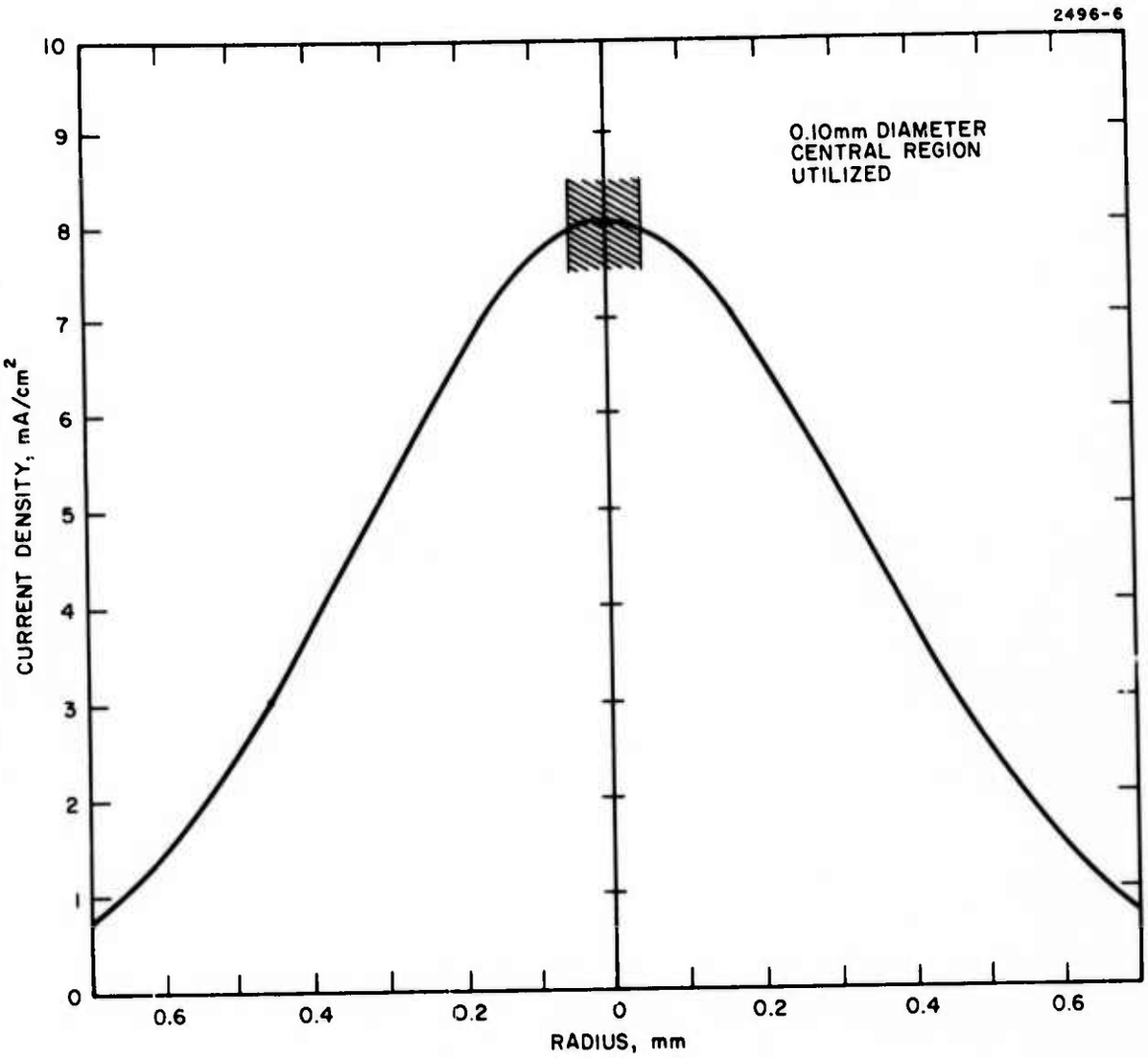

Fig. 10. Calculated current density as a function of radius for cathode temperature of 0.32 eV and 0.325 mm cathode diameter at the crossover. By using only the central region of the beam, only the full brightness of the source may be preserved in the beam waist.

electrons which are generated along with the negative ions. The additional space charge created by these electrons, which are inevitably produced along with any negative ion beam, must be considered in the design of any negative ion extraction system.

Since virtually no experimental data was available at the onset of this program, the design of the negative ion source was considerably more complicated and speculative than that of the cesium source. First, an experiment was necessary to verify the analytical predictions presented in the proposal. Second, an ion optical design was necessary to form the negative ion beam while simultaneously controlling the additional space charge created by the electrons which are mixed with the negative ions. Finally, a mechanical design which incorporated all of the necessary mechanical features within the constraints imposed by the rather difficult LaB_6 technology was required.

Because of the relatively brief period available to complete Phase I (90 days), the above three activities were of necessity conducted in parallel rather than in series. The result (particularly in the ion optical study) is that the results are presented parametrically and that the final operating point for the prototype source will be chosen as the detailed design proceeds in the initial part of Phase II which is currently underway as this report is written.

a. Ionization of Iodine on LaB_6 – The principle objective of this experiment was to demonstrate the feasibility of a contact ionization negative ion source. The specific goals were to demonstrate the formation of negative iodine ions on a lanthanum hexaboride (LaB_6) surface, to measure the electron to ion current ratio and to determine the ion current density at the emitter surface. Typical goals, for these values generated in a study, of the ion optics requirements has shown that a desired design goal would be for the negative ion source to operate at an ion current density of 5 mA/cm^2 and at an electron to ion current ratio of less than 1000.

The demonstration tests were performed using a high field-point geometry ion source. Although this source geometry is not the optimum for this test, the preliminary results demonstrated the formation of a significant negative ion current. The ion current density was estimated to range from about 0.2 to 2.4 mA/cm^2 with the electron to ion current ratios (f) varying from about 500 to 5000.

The selection of a contact ionization system for a negative source was based on the requirements for high brightness, high efficiency and low gas load. Electron attachment in the gas phase is inherently a very inefficient process. These considerations are discussed in detail in the technical proposal presented for this program.

LaB_6 was chosen as a cathode material on the basis of its work function, operating temperature range, and resistance to poisoning. By means of the Saha-Langmuir equation, it is possible to show than an LaB_6 cathode is capable of operating at a 75% efficiency. Previous studies have indicated that the operation of the LaB_6 cathode at about $1700^{o}K$ results in essentially total dissociation of the I_2 molecules to form I^- ions.

The I_2-LaB_6 system does present severe material compatibility problems which were considered in the design of the source. The iodine gas is reactive with most metals resulting in the formation of volatile metal-iodide compounds. These gases decompose on heated surfaces resulting in the deposition of the metals onto heated surfaces. As a result, much care must be used in designing the I_2 vapor feed system and the ion source chamber to prevent the deposition of metals over the heated cathode (which would poison the cathode). Because boron diffuses out of LaB_6 when it is in contact with metal structures at high temperature, resulting in a destruction of the LaB_6 and the support structure, it is necessary to design a cathode which is supported at its cool end.

2. Experimental Apparatus

The ion source chosen for this study was adapted from an existing high field-point geometry electron gun design. This is shown in Fig. 11 in a cross-sectional view. The point cathode is

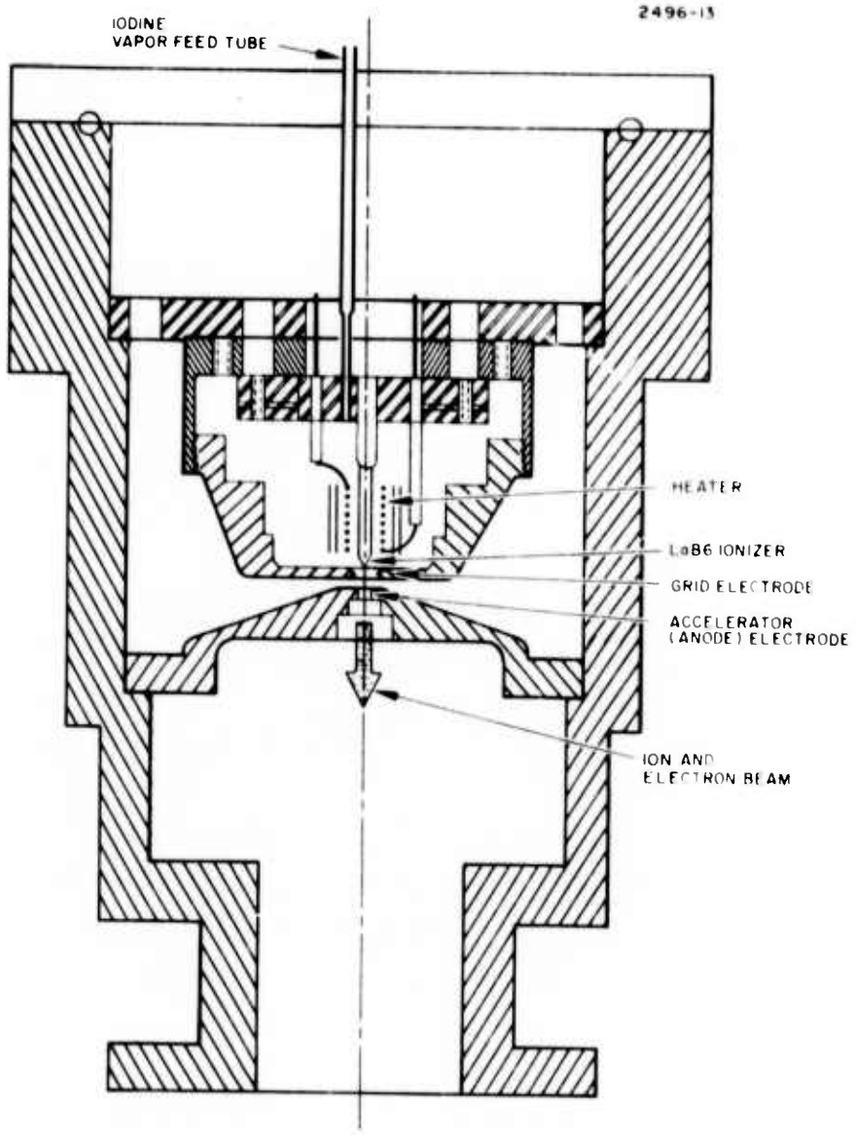

Fig. 11. Cutaway view of the high field-point geometry ion/electron source. The LaB_6 rod cathode, the spiral tungsten wire heater and the heat shields are mounted on an Al_2O_3 plate. This unit is contained inside the grid assembly which is mounted on an Al_2O_3 plate that locates this unit with respect to the grounded anode. The iodine vapor feed tube delivers the iodine with the chamber formed by the grid assembly.

mounted inside the grid electrode. These are positioned with respect to a grounded anode electrode. Iodine gas is admitted to the interior of the grid. The negative ions and electrons formed in the cathode are accelerated through the anode into the vacuum chamber. A transverse magnetic field is used to deflect the electrons from the ion beam. The electron and ion currents are measured by means of a shielded Faraday collector. The cathode temperature is determined by means of a disappearing filament micro-optical pyrometer.

The cathode is an LaB_6 rod that is 15-mm long and has a 1 by 1 mm square cross section. The tip of the cathode is ground into a 90^o conical point. The base of the cathode is brazed into a copper support post. It is positioned 275 μm behind the face of the grid. The cathodes are manufactured by Cambridge Instruments for use in the scanning electron microscopes.

The cathode is radiation and electron bombardment heated by means of a spiral tungsten heater which surrounds the cathode. The heater is enclosed in a three-element heat shield which is made from rhenium foil. The heat shield is held a heater potential thus optimizing the electron bombardment of the cathode. These components are mounted on a Al_2O_3 ceramic base.

The cathode assembly is enclosed within a stainless steel grid cap. The grid is operated at a negative potential with respect to the cathode thus restricting the cathode emission to a small area of the tip. The grid cap also confines the iodine vapor to the cathode region.

The cathode and grid units are mounted on an Al_2O_3 ceramic plate which electrically isolates the cathode and grid from ground potential and locates and positions these with respect to the anode. The grid to anode gap is 3.13 mm. The isolator plate is machined to a tolerance of 12 to 25 μm of the chamber wall, thus permitting the accurate assembly of these gun elements with respect to the anode. The selective positions of these electrodes is shown in Fig. 12.

The iodine vapor is transmitted into the cathode region by means of a quartz tube which is attached to an external iodine reservoir. The flow of iodine gas into the chamber is controlled by the

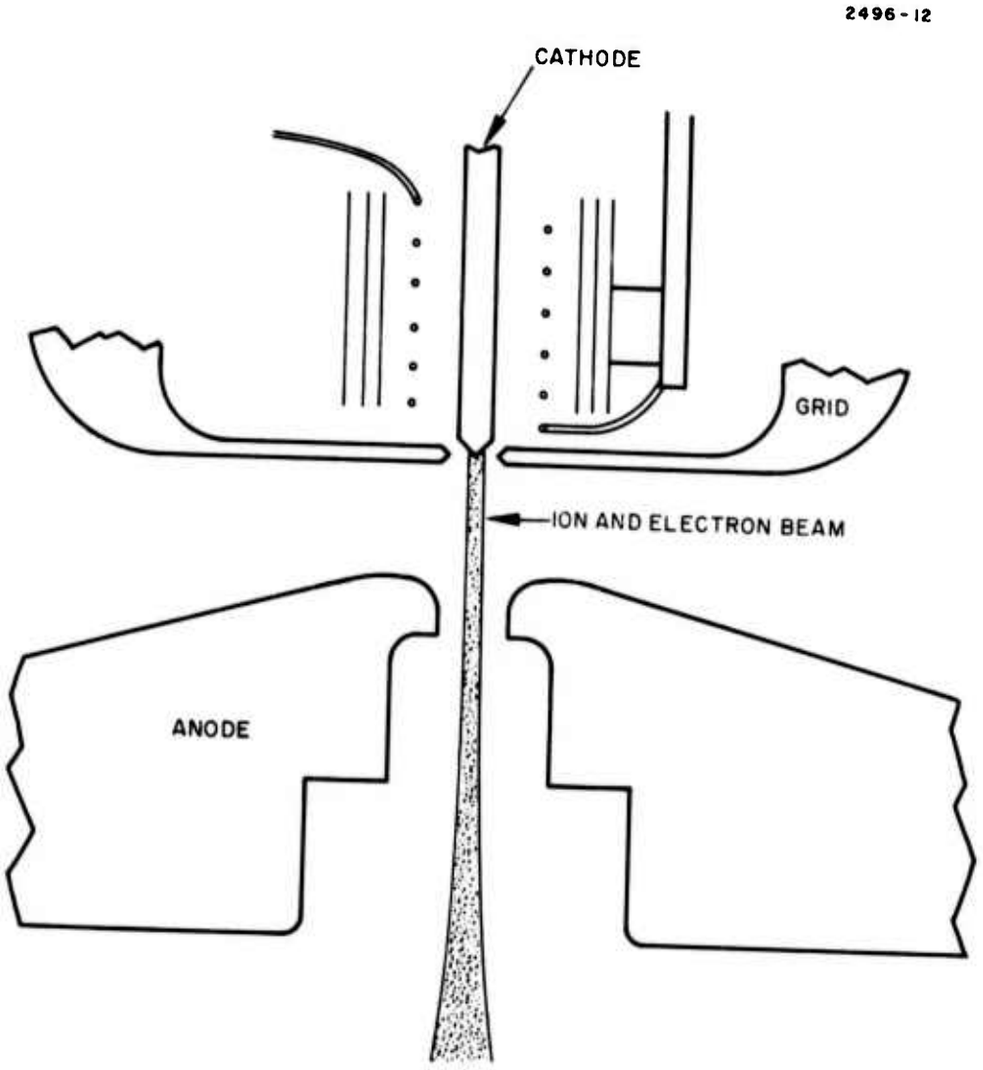

Fig. 12. Enlarged cross-sectional view of the cathode-grid-anode region. This shows the relative position of each electrode.

temperature regulation of the external iodine reservoir by means of a constant temperature bath. The bath is regulated to 0.1°C which corresponds to a change of less than 1% in the iodine vapor pressure.

The combined ion-electron beam is accelerated through the anode electrode into the vacuum chamber. The beam is sufficiently narrow that a 6.2 mm diameter Faraday collector, located 25 cm from the anode, collects about 10% of the total beam. The Faraday collector is totally shielded except for the entrance aperture. The collector has a length-to-diameter ratio of 4 which insures that secondary electrons do not contribute to the measured currents. The Faraday collector is mounted on a sliding seal which makes the scanning of the ion/electron beam possible.

The electron beam is separated from the ion beam by means of a transverse magnetic field. This is shown in Fig. 13. A permanent magnet is used to produce a field of 260 ± 10 G over a 6 cm ion-electron path length. This field is adequate to separate the electrons from the ion beam with negligible deflection of the ion beam.

A quartz window coated with a conductive coating (to prevent charge buildup) is located at the end of the chamber behind the Faraday collector. Observations are made through this window (by means of a brightness pyrometer) to determine the cathode temperature.

The electrical circuit is shown in Fig. 14. The cathode bias (V_B) is provided by either a Fluke 410B power supply or a Power Design HV1579R power supply. Both are regulated to 0.001%. The grid bias V_G is developed from a series of dry cell batteries. The electron bombardment heater bias V_H is obtained from a Harrison 6209B power supply operated in a constant current mode. The total emission current I_A is the combined anode, chamber and Faraday collector shield currents. It is equal to the current through the cathode bias power supply. The Faraday collector current I_{FC} is measured by means of a Keithly 410B electrometer.

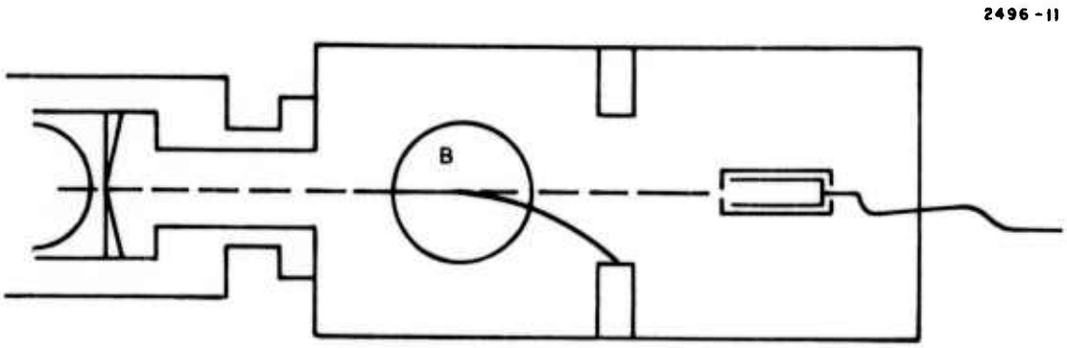

Fig. 13. Cross sectional view of the test chamber showing the separation of the electrons from the negative ions.

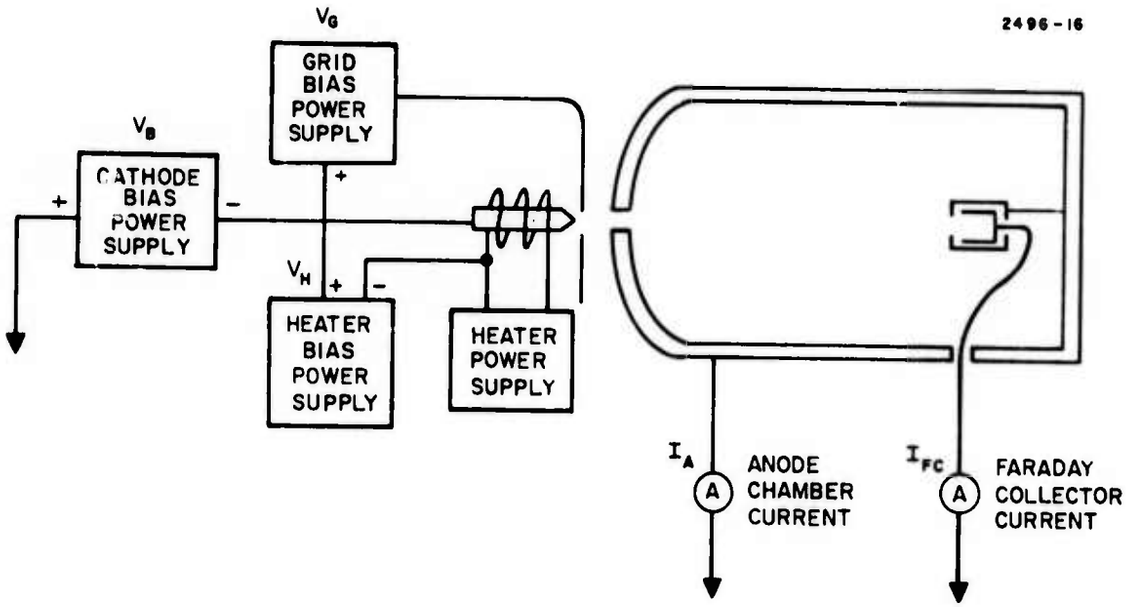

Fig. 14. Schematic of circuit used in tests. The accelerating potential is provided by the cathode bias power supply. The grid is biased negative with respect to the cathode to restrict emission to the tip of the cathode. The cathode is heated both by radiation and electron bombardment heating. The total emission current (less the Faraday collector current) is measured as the anode/chamber current.

3. Experimental Procedure and Results

The first step in the operation of the ion source was to determine the characteristics of the radiation/electron bombardment heating of the cathode. These measurements were made with the cathode and grid – a ground potential.

The next step was to gradually increase the potential of the cathode and grid (with the heater turned off) until the system could withstand the maximum potential without arcing.

Electron emission measurements were then made as functions of cathode temperature, cathode bias, grid bias, and Faraday cup position. In addition to verifying the operation of the apparatus, these tests were necessary to establish the activation of the LaB_6 cathode. The initial operation of a new cathode requires heating to 1700°K to activate the cathode. This is demonstrated by determining the work function of the cathode by means of a plot of log I_{FC}/T^2 as a function of $1/kT$, where I_{FC} is the electron current measured by the Faraday collector and T is the cathode temperature in degrees Kelvin. In this study the LaB_6 cathode exhibited a work function of 2.9 ± 0.15 eV which is in reasonable agreement with the literature values.

The magnetic deflection system for removal of the electrons from the ion beam was tested at this time. A small negative ion current was observed. It is most probably due to OH ions formed on the cathode from the residual water vapor. The magnitude of this background negative ion current is 1% or less than the iodine negative ion current obtained after the admission of iodine to the system; thus, the background current is negligible.

Introduction of iodine gas resulted in the generation of a significant negative ion current. Most of the measurements were made in the temperature range of 1650 to 1750°K. A limited number of observations were made down to 1628°K and up to 1890°K. Because of the source design limitations, it was not possible to establish the absolute iodine arrival rate. As the vapor pressure of the iodine in the external reservoir was varied from 0.115 to 0.278 ton, the arrival rate at the cathode should have varied accordingly.

For a fixed iodine arrival rate, one would expect the electron to ion ratio to increase as the cathode temperature increases. This is a consequence of the fact that the iodine vapor flow is fixed but the electron emission is temperature dependent. A typical example is shown in Fig. 15. A summary of all the data shows the electron to ion ratio to be about 500 to 700 in the temperature range of 1630 to 1670°K; 700 to 1800 in the range of 1680 to 1750°K; and 1000 to 5000 above 1750°K.

The ion current density at the LaB_6 surface was estimated in the following manner. It was assumed that the electron and ion beam trajectories are identical; thus, the current of each species which was measured in the Faraday collector is estimated to be generated from the same surface element of the cathode. The LaB_6 surface was assumed to have a work function of 2.9 eV. For each cathode temperature, the Richardson equation ($J = AT^2 \exp - \phi kT$) was solved to determine the electron emission current density Joule. Using this value and the electron current measured at the Faraday collector, it was possible to calculate the area which generated the electron current. This calculated surface area was applied to the observed negative ion current to determine the ion current density at the cathode.

About 70% of the calculated ion current density values are in the range of 0.2 to 1.0 mA/cm^2; the remainder are below 2.5 mA/cm^2. There does not appear to be any temperature dependence associated with these values. The accuracy of this estimate is believed to be within a factor of 2. This is based on the following analysis: for an increase of 0.1 eV in the work function assigned to the LaB_6, the calculated ion current density decreases by a factor of 50%. As the electron currents observed before and after the admission of iodine (for cathode temperature about 1700°K) are nearly equal, it is unlikely that the surface electron work function was changed much from the 2.9 eV value.

4. Negative Iodine Ion Extraction System Design

As described above a surface ionization technique is able to produce negative iodine ions with the necessary current density and thermal energy to permit extraction of an ion beam with the desired brightness of 100 A/cm^2 sr. Since these current density values are

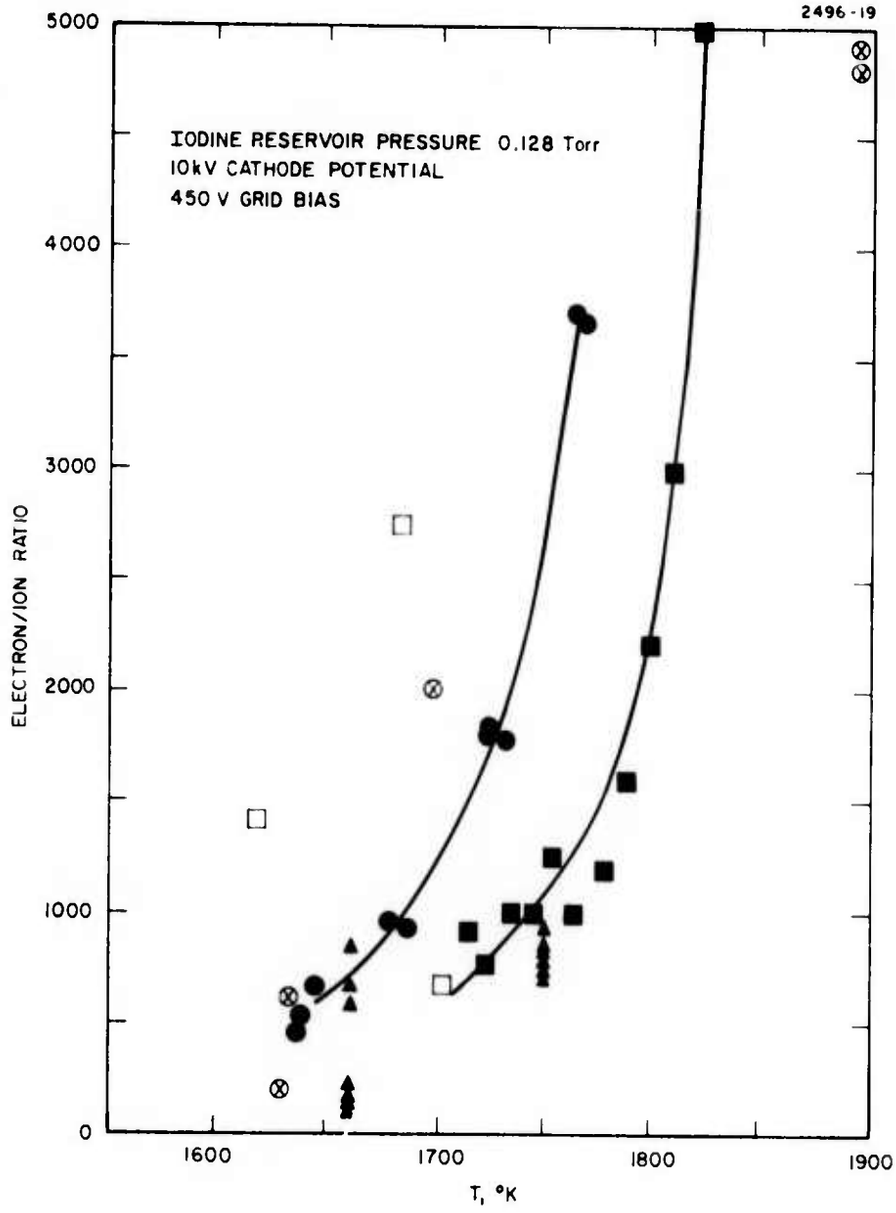

Fig. 15. Plot of electron to ion current ratios as a function of cathode temperature. At a constant iodine gas arrival rate, the electron/ion ratio should increase as the temperature is increased. Two such cases are indicated by lines. The other cases were obtained at varied iodine flow rates and fixed cathode temperatures.

two orders of magnitude above the current density values reported in the literature, the extraction system design was conducted parametrically while this data was collected in a parallel experimental program. The assumed boundary conditions are similar to those used for the cesium ion computation, i.e., 20 kV beam voltage and 0.32 eV thermal energy. This requires an emission current density of 5 mA/cm^2 for the 100 A/cm^2 sr brightness.

The primary difference between the design of cesium and iodine ion extraction geometries relates to the requirement to account for the space charge of the electrons which are emitted along with the negative iodine ions. It is, therefore, convenient to define a total equivalent electron current I_{equiv}, for a given iodine current I_- and electron current I_c by

$$I_{equiv} = I_- \sqrt{\frac{M_{ion}}{m_e}} + I_e \quad . \tag{2}$$

Letting the ratio of the electron to iodine current be defined as $f = f_e/I_-$ eq. (2) can be written (since $\sqrt{M_{ion}}/m_e \cong 482$ for iodine) as

$$I_{equiv} = I_- (482 + f) \quad . \tag{3}$$

Since $I_- = J_- A_{cath}$ and J_- has been fixed at 5 mA/cm^2 from the brightness requirement, eq. (3) can be rewritten to relate the total equivalent electron current and the effective cathode size as

$$I_{equiv} = (5)\ \pi/4\ (d_{cath})^2\ (482 + f)\ mA \quad . \tag{4}$$

This relation has been plotted in Fig. 16 for electron to ion ratios of 10 $\sqrt{M}/m_e$ (~5000), $\sqrt{M}/m_e$ (~500) and zero. These values cover the range from a worst case condition where the electrons completely dominate the space charge ($f \approx 5000$) to the opposite extreme where no electrons are emitted ($f = 0$). The intermediate case ($f \approx 500$) in which the electron and ion space contributions are equal is also shown. The equivalent electron current calculated above has been converted to the equivalent electron perveance at 20 kV as follows:

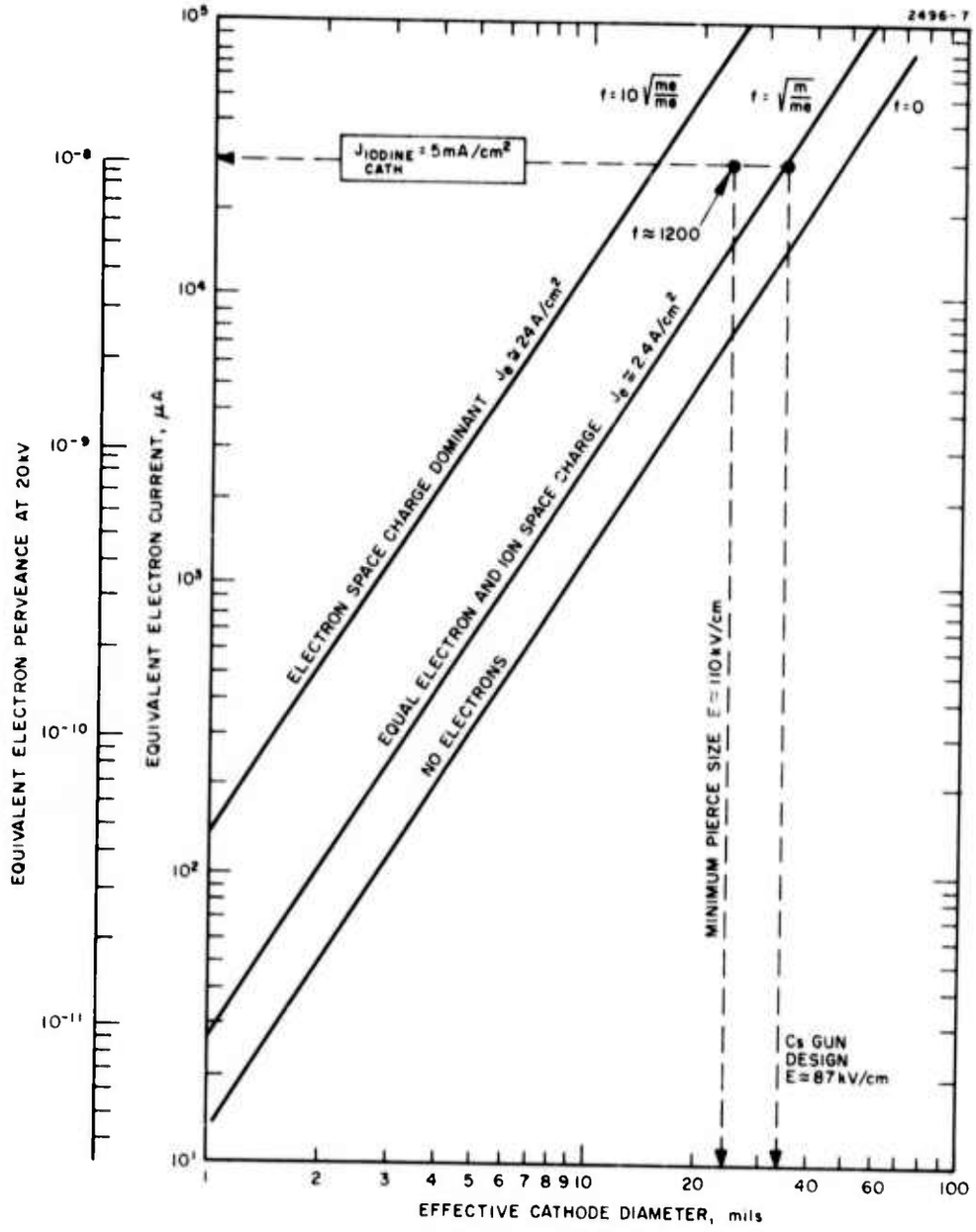

Fig. 16. Equivalent electron current and perveance as a function of effective cathode diameter for different electron to iodine current ratios f. For a given current the cathode diameter becomes impractically small for large electron to ion ratios.

$$P_{equiv} = I_{equiv}/(20,000)^{3/2}\ A/V^{3/2} \quad . \qquad (5)$$

This equivalent electron perveance is shown as another vertical scale on Fig. 16.

The gun design is extremely dependent on the f value because the required perveance for a given scale (cath size) is uniquely determined once this parameter is fixed. Alternately, once a gun design is fixed and the perveance is known, the scaling (cath size) can be changed to supply the required current density determined by the f value subject to voltage breakdown and fabrication constraints. Thus, the perveance, scaling and f value are interrelated and must be self-consistent to achieve the desired brightness.

a. Pierce Gun – The Pierce Gun design for the Cs ion source would be directly applicable to the I^- source if the experiments in progress shown that (1) thoriated tungsten is an efficient I^- producer and (2) the f fraction is equal or less than ~500. In this case the porous tungsten ionizer would be replaced by a thoriated tungsten wire bundle and the cesium feed system would be replaced by an iodine feed system. Reference to Fig. 16 shows that a perveance 10^{-8} gun structure with a 0.85 mm diameter cathode is on the $f = \sqrt{M}/m_e\,(500)$ line. In this mode of operation $I_{iodine} \cong 27\ \mu A$, $I_{electron} = 27 \times 482 \cong 13$ mA and the mode of operation is completely equivalent to a Cs operating point of 57 μA. That is, the optics, trajectories, etc., would be exactly the same for the latter condition. If it turned out that f was less than 500, this geometry could be scaled up in size to accommodate the lower current density requirement. Thus, at f = 0 the 5 mA/cm^2 of I^- would be accomplished with an ionizer diameter of 2 x .85 = 1.70 mm. In this case, $I^- \cong 57\ \mu A$ and again we have a situation where the optics are identical to cesium extraction at 10 mA/cm^2.

To use this Pierce Gun design for f > 500, it follows from Fig. 16 that the cathode diameter and all other dimensions would have to be scaled down in size. The description of the cesium gun design

shows that for a 0.85 mm diameter cathode configuration the maximum electric field is ~87 kV/cm, which increases to ~107 kV/cm for a 0.67 mm diameter cathode configuration. From practical fabrication and voltage breakdown considerations this is about as small a Pierce geometry as is feasible. If this configuration could be built it would handle a f ratio of $2 \times \sqrt{M}/m_e \cong 1000$. Any higher f values lead us to consider point cathode or hairpin type of electron guns.

b. Point Cathode Guns – Higher electric fields than are attainable at the flat or concave emitter of a Pierce Gun can be achieved by employing a sharply pointed emitting surface. The point cathode or hairpin type of gun is a three element gun which is characterized by low perveance ($\sim 10^{-10}$ $A/V^{3/2}$) high electron brightness and very small cathode diameter 0.0005 cm to 0.005 cm. These types of guns have been used for many years in applications where tens to hundreds of microampere electron beams of small angular divergence have been required, such as electron microscopes and SEMS. Although many investigators[3-6] have made detailed experimental studies of these types of guns, there is no unified theory or design procedure analogous to the well known design procedure for the Pierce type of gun. To our best knowledge these guns have never been employed for ion extraction. Most of the understanding of the point cathode electron gun has been based on empirical performance data. The two main types of point cathode guns are the "short focus" and telefocus. In the short focus gun the crossover is formed between the cathode and anode and an external condenser lens is used to image this internal crossover, which is quite small, typically 0.01 to 0.05 mm. In the telefocus type the crossover is formed 10 to 30 cm downstream of the anode and is typically 0.4 mm in diameter. Examples of these two types of guns along with their measured brightness, beam angle, etc., are shown in Figs. 17 and 18. It is seen that the highest electron brightness is respectively 1.5×10^5 and 5×10^4 A/cm^2 sr for the short focus and telefocus types. There is another variation of the short focus type in

0-2496-24

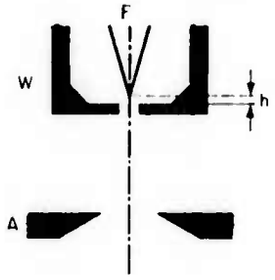

0-2496-25

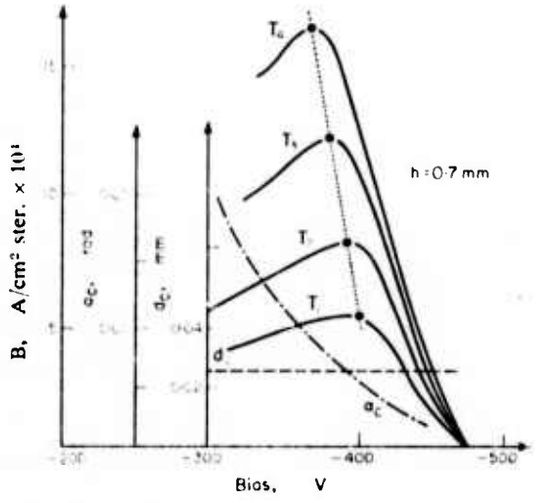

Fig. 17.
Schematic and typical characteristics of short-focus hairpin filament gun (from Ref. 4).

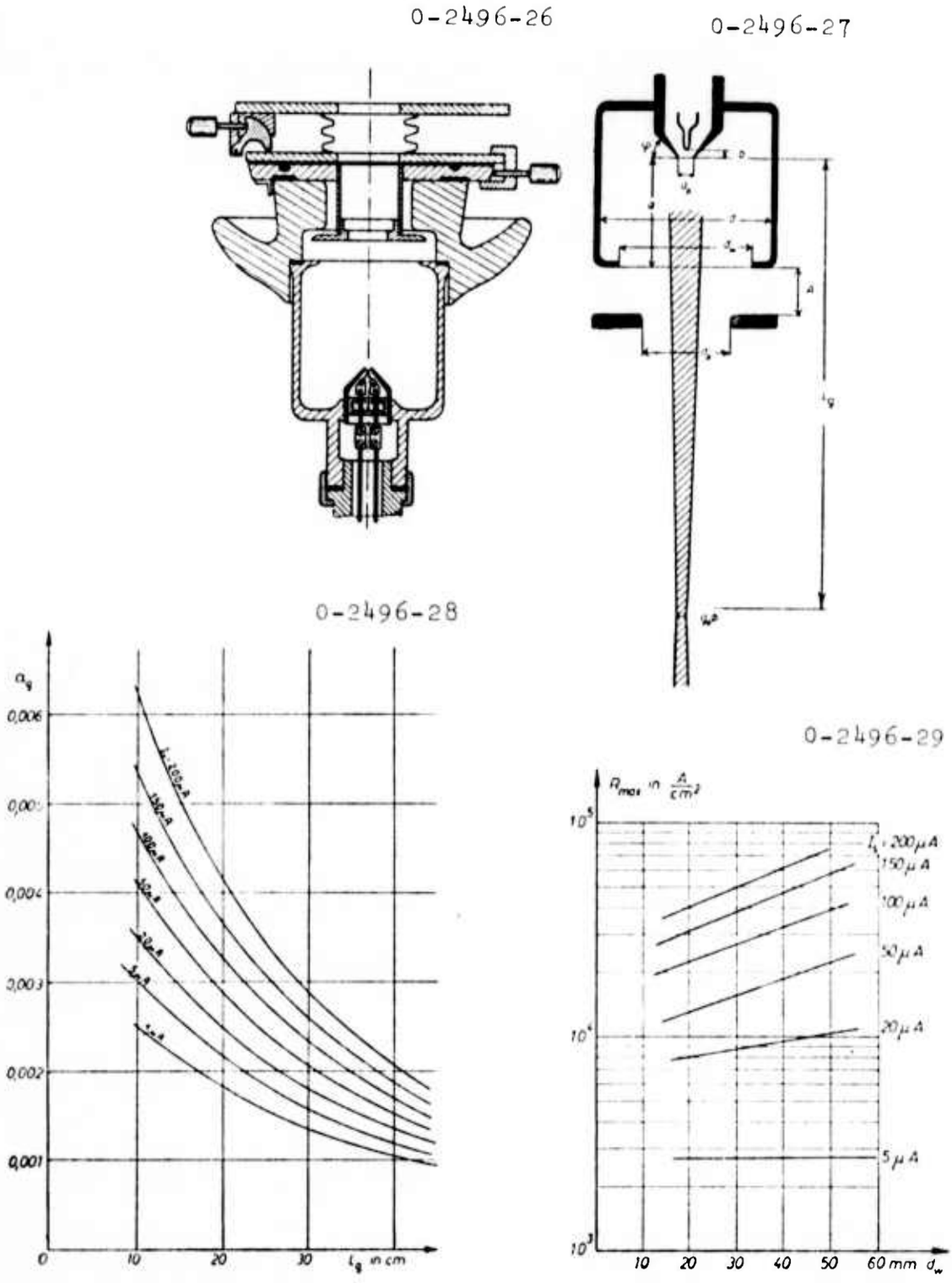

Fig. 18. Schematic and typical operating characteristics of tele-focus type gun (from Ref. 5).

which a very sharp (< 100 μ) LaB_6 tip is used instead of a hairpin, in a geometry similar to that shown in Fig. 17. Reference 6 has reported electron brightness of up to 10^6 A/cm^2 sr for this type of gun. A version of this type of gun has been used at HRL for electron beam recording and has been used for the experiments on I^- generation. A schematic of this gun, along with some trajectory calculations for two different cathode positions, is shown in Fig. 19. The actual point cathode type of gun chosen for the I^- source depends on the electron to ion ratio f. The reduction in I^- brightness as this ratio is increased from ~10 to ~5000 is shown in Fig. 20 for initial electron brightnesses typical of these guns. Thus, Fig. 20 showing a gun design based on the telefocus version would have the required brightness of 100 A/cm^2 sr at f = 0 but would decrease to an I^- brightness of 20 A/cm^2 sr at f ≈ 2000. The short focus gun type as shown in Fig. 17 would have the required 100 A/cm^2 sr I^- brightness up to an f value of 1000. However, a condenser lens would probably be required to match this gun to the AMS.

The above computations illustrate that the relatively large electron to ion ratios expected from the LaB_6 surface are not as difficult to control as might be initially expected because an electron, being much higher than an ion only contributes 1/500 as much to the space charge as the ion. Therefore, an electron to ion ratio of 1000 will require an extraction system perveance of a factor of three greater than an equivalent positive ion gun. This represents a practical upper limit which might be extended another factor of two by careful design if the experiments prove it necessary.

5. Summary of Iodine Source Design

As a result of the favorable electron to ion ratios observed experimentally (i.e., f < 1000), it is possible to use a Pierce ion gun geometry similar to that used in the cesium source. This is a very desirable result because this type of system is well understood and has been accurately modeled for computer simulation of the ion trajectories. It should, therefore be possible to design an electrode structure which will produce the necessary bright beam with a minimum number of experimental perturbations. Such is not the case for the point cathode sources for which only empirical parametric studies are available.

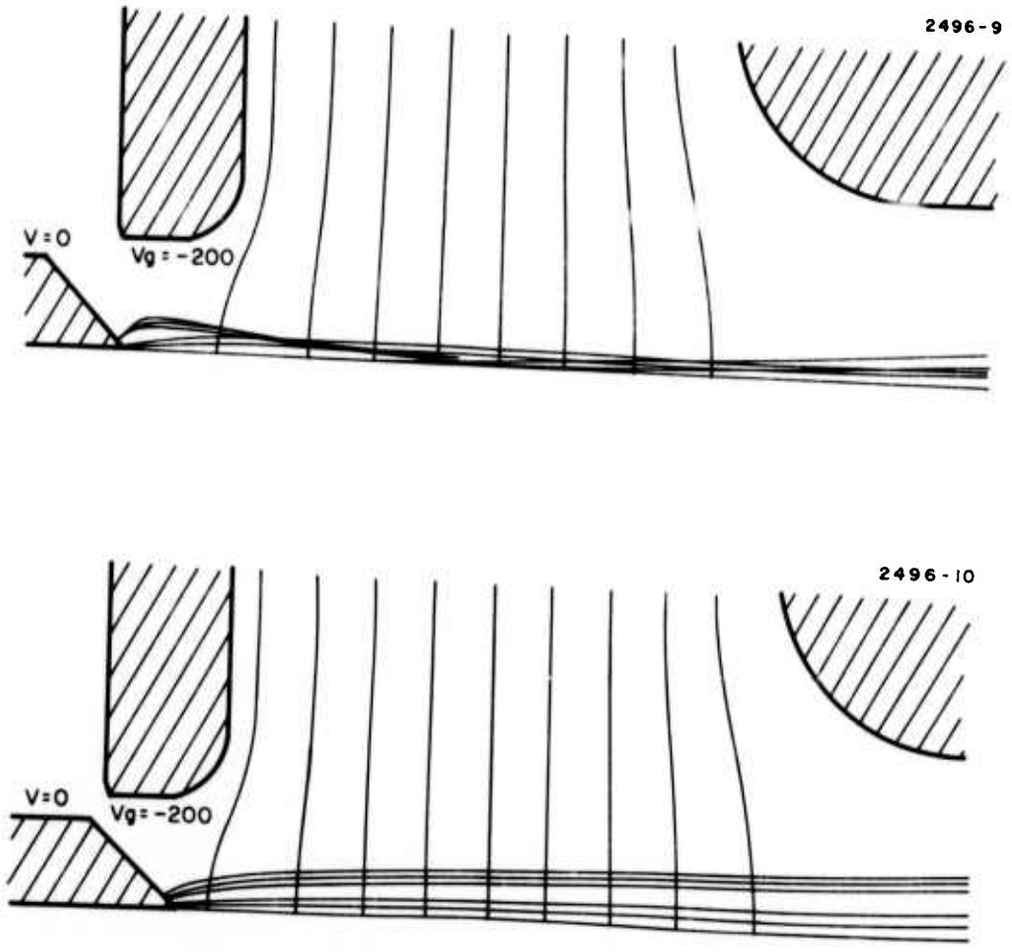

Fig. 19. Computer trajectory calculations for Hughes Research Laboratories point cathode gun design for two cathode positions. Note increase in trajectory crossovers as the emitter is moved upstream.

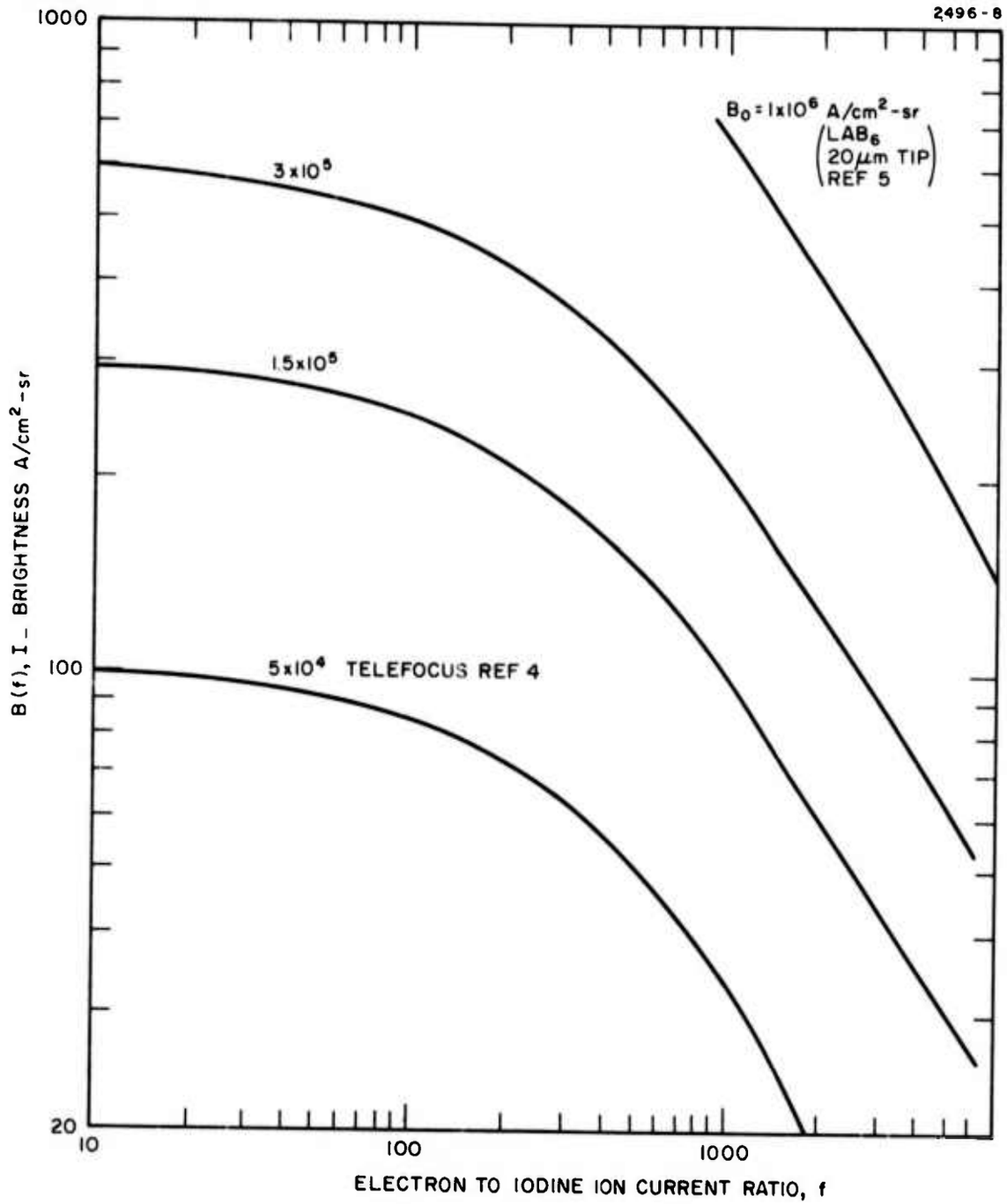

Fig. 20. Graph showing decrease in effective I-brightness as a function of electron to ion ratio f for different point cathode type geometries. The brightness values shown on the curves were measured in experiments with only electron emission.

Negative ion current densities of 20 to 40% of those required in the final device were measured. In view of the brief experimental period and the fact that these current densities are two to three orders of magnitude greater than any previous by reported values, this is also a very encouraging result. A high confidence factor is placed on our ability to produce the required brightness in a fully optimized system.

C. Prototype System Design

1. Cesium Ion Source

The cesium ion source layout, shown in Fig. 21 describes the basic construction of the source. The Pierce design ion optics electrodes, ionizer assembly, and feed system are attached to the main mounting flange. The focus electrode is supported by three high alumina (99.8% Al_2O_3) insulators approximately 2.0 in. long. Clean alumina insulators of this design have the capability of holding off 50 kV in vacuum. The focus electrode is made of vacuum grade pure molybdenum to resist sputtering by backstreaming ions or electrons. The anode, or downstream electrode, is made of OFHC copper which has been shown to re-evaporate from the emitting surface if sputtering of this electrode takes place. The anode is supported from the mounting baseplate by three 304 stainless steel posts since the electrical potential is the same. The electrodes are fabricated to close tolerances and all corners rounded and electropolished to a very high finish to reduce electrical breakdown at the operating voltage level of 20 kV.

The cesium ion emitter is a porous tungsten plug 0.087 cm diameter by approximately 0.15 cm long, made from 4.0 μm spherical tungsten powder, pressed and sintered to 80% density to produce approximately 3×10^6 pores/cm^2, each 2.0 μm in diameter. The porous tungsten plug is mounted in a solid tungsten body 0.3 cm diameter which in turn is attached to a thin walled moly-rhenium feed tube to reduce thermal conduction along the length of the tube. The feed tube is attached to a flange to provide a convenient interface with the mounting base-feed system reservoir. The ionizer, feed tube, and flange

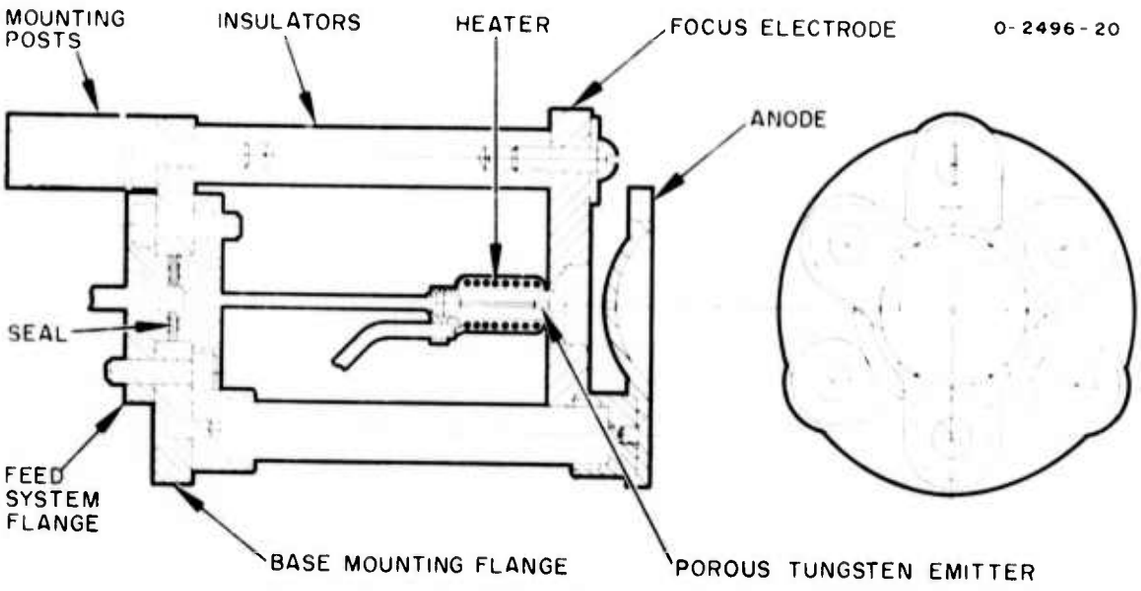

Fig. 21. Layout of cesium ion source.

are assembled by standard electron beam welding (EBW) techniques to provide a leakproof integral subassembly. The ionizer tip is heated with a plasma sprayed (alumina) heater, shown in Fig. 22, using tungsten-rhenium heater wire. This heater fabrication technique has been developed at Hughes Research Laboratories for use as cathode heaters on ion bombardment thrusters and operates successfully at temperatures up to 1200°C.

The feed system reservoir is attached to the ionizer assembly by a demountable, crush seal flange which utilizes an annealed metal washer between clamped surfaces to provide a leak-proof replaceable seal. The feed system also is equipped with a small solenoid valve in the feed line to allow the cesium reservoir to be sealed off when not in operation or for removal from the vacuum enclosure.

The complete ion source assembly is mounted to the positioning mechanism by three stainless steel posts. An electrical schematic of the cesium source is shown in Fig. 23.

2. Negative Iodine Source Mechanical Design

The basic mechanical construction used for the negative ion source is the same as that previously discussed for the cesium ion source. The primary differences between the designs lie in the vapor feed schemes, emitter materials and heating technique. The emitting surface is lanthanum hexaboride (LaB_6) which is a brittle, crystalline material having similar thermal and electrical properties to refractory metals and is an excellent electron emitter. In order to produce iodine negative ions, iodine vapor must be present at the surface and this can be accomplished by one of the three basic methods described in the following paragraphs.

Iodine vapor is fed into the emitter area by an annular groove in the focus electrode as shown in Fig. 24. The flange and feed tubes are attached to the two-piece focus electrode by EB welding the assembly together and attaching to the feed system reservoir in the manner previously presented. The LaB_6 rod is attached by brazing or mechanical attachment to the flange to be developed during the next phase of this program.

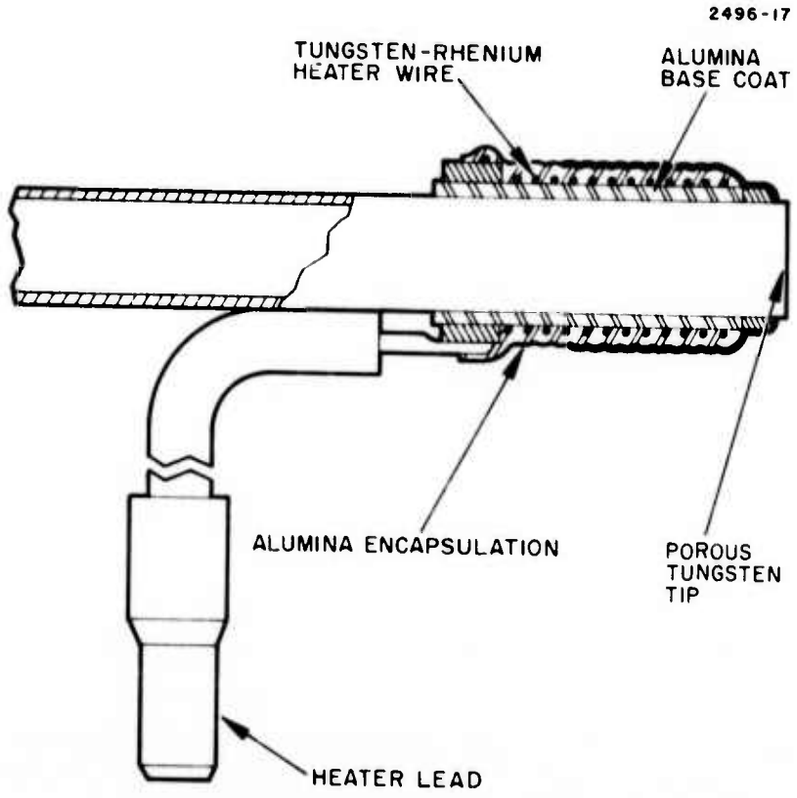

Fig. 22. Plasma sprayed cathode heater.

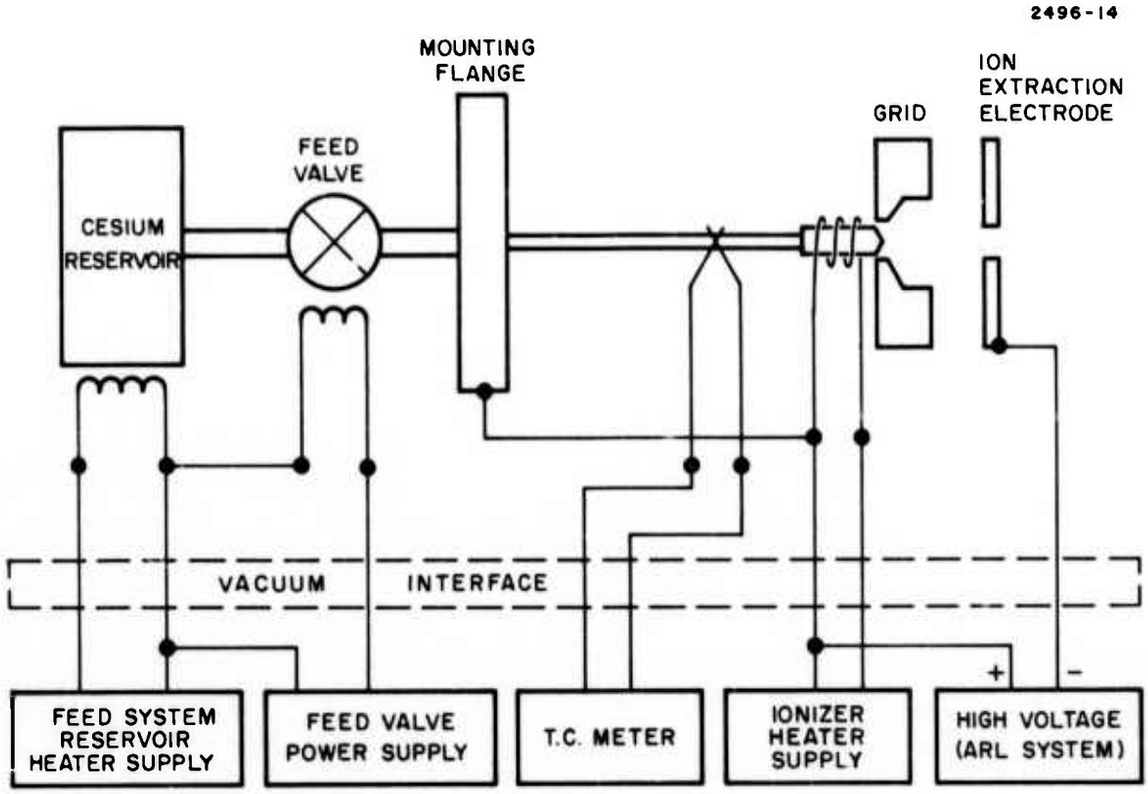

Fig. 23. Electrical schematic of cesium ion source.

2496-16

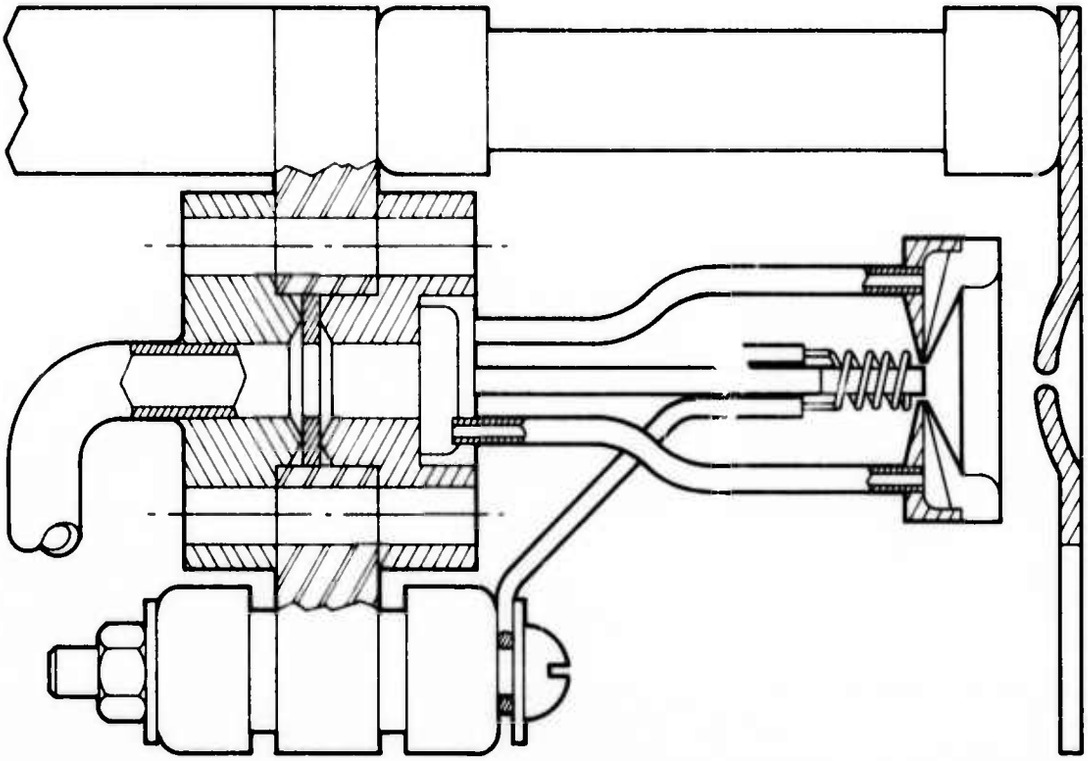

Fig. 24. Schematic of iodine source. Note the electron bombardment heater and iodine vapor feed system described in the text.

Another method under consideration is to feed the iodine vapor through a small tube of hypodermic size which is located in the focus electrode near the downstream end of the angled surface. The tube is directed so that the iodine is "sprayed" onto the emitting surface. Details of this design have not been worked out at this time.

Another interesting concept of vapor feed which makes the overall source design simpler and more workable is to fabricate an ionizer assembly similar to the porous tungsten design used in the cesium source. A porous LaB_6 rod can be used and backfed through a hollow core. The inherent properties of LaB_6 rods make this concept appear to be feasible since LaB_6 is manufactured by the supplier in theoretical densities of 70 to 95% and appears to have the proper porosity and mechanical strength for this application as determined by preliminary testing at HRL. The outside surface of the tube can be sealed tc prevent vapor flow through the walls by electron beam "washing" of the surface. Again, preliminary tests have shown this method to be feasible. An alternative method is to captivate a small porous plug of the proper density in a rhenium or other nonreactive tube such as used in the cesium source design.

As mentioned previously, the heating method of the negative ion source is different from the cesium source since the temperature limit of plasma sprayed heaters is below the anticipated operating temperature of the iodine source at approximately 1500°C. The LaB_6 rod is heated primarily by an isolated bare heater wire of tungsten and additional heating is provided by electron bombardment of the rod by using an additional heater bias power supply. The electrical schematic of the negative ion source is presented in Fig. 25.

3. Source Positioning Mechanism

A basic requirement of the overall system design is the capability to position either of the two operating sources within a tolerance of ± 0.002 cm relative to the downstream ion column. A rotating assembly shown in Figs. 26 and 27 has been designed to accomplish this purpose. It consists basically of a large hollow shaft supported

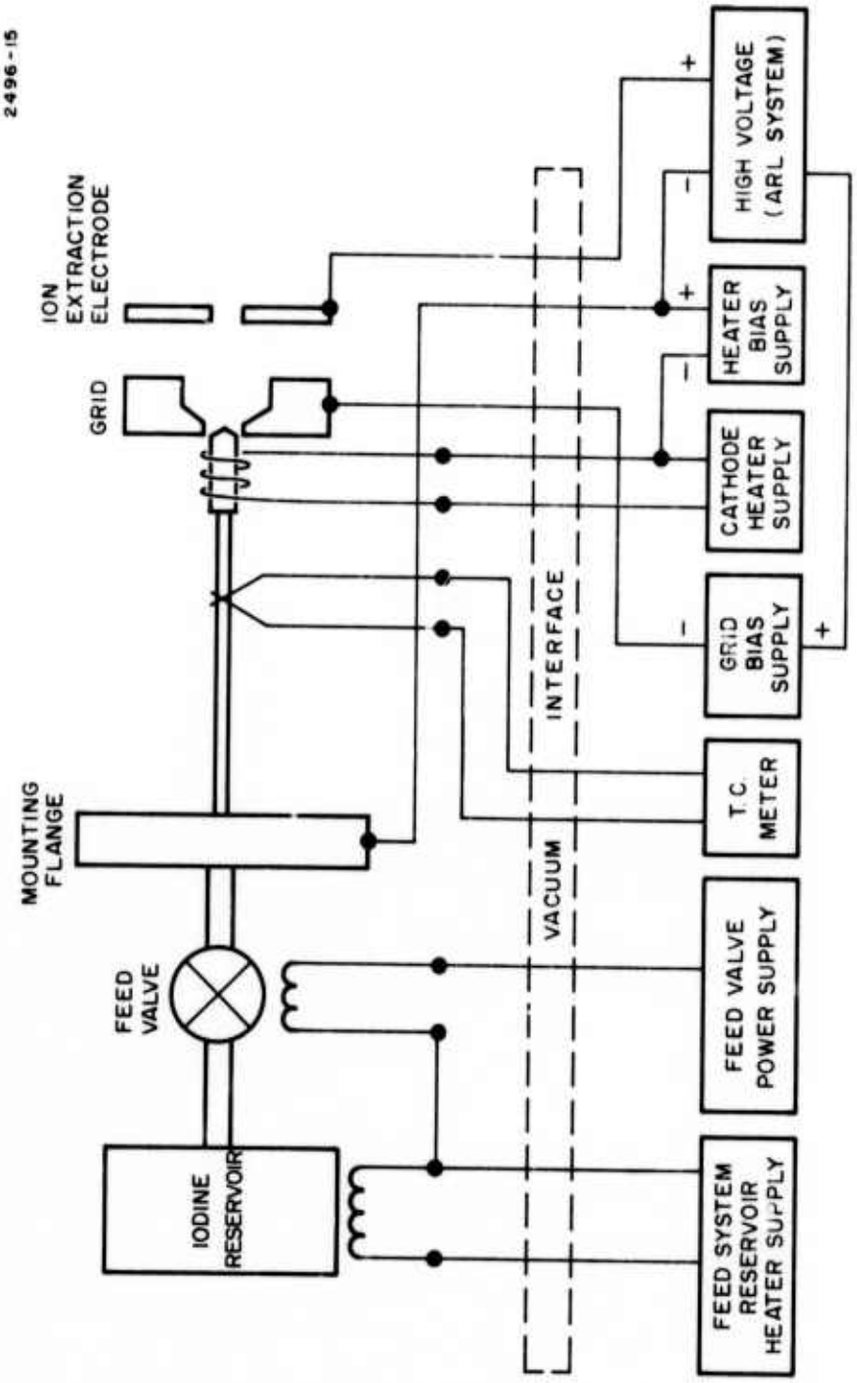

Fig. 25. Electrical schematic of negative iodine source.

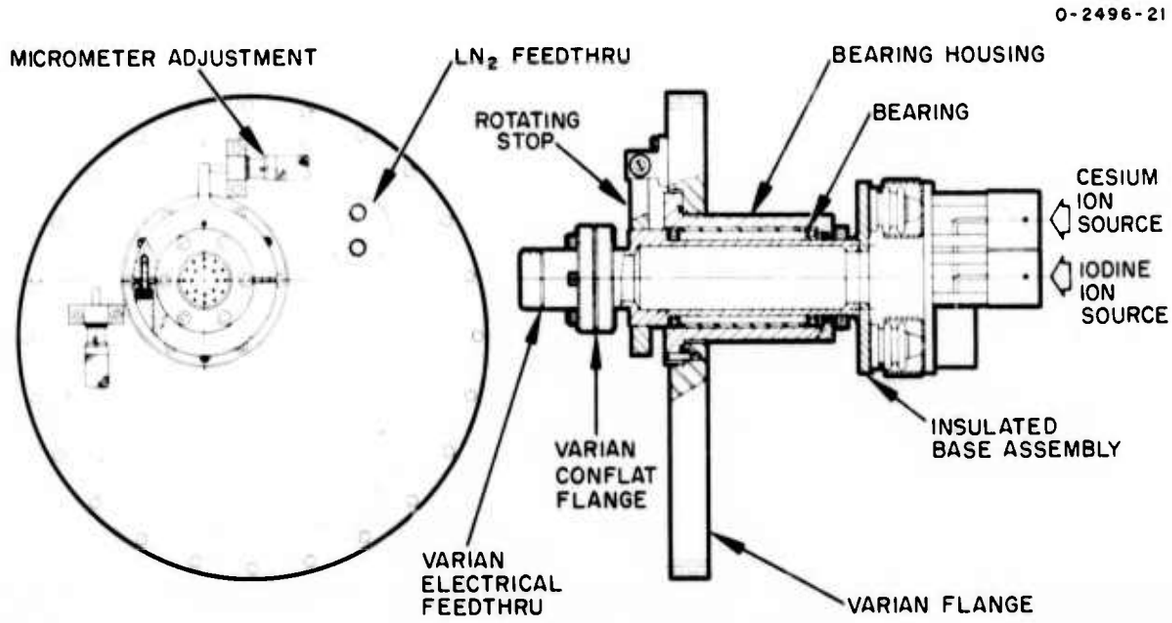

Fig. 26. Detail of rotating assembly used to reposition cesium or iodine sources.

0-2496-23

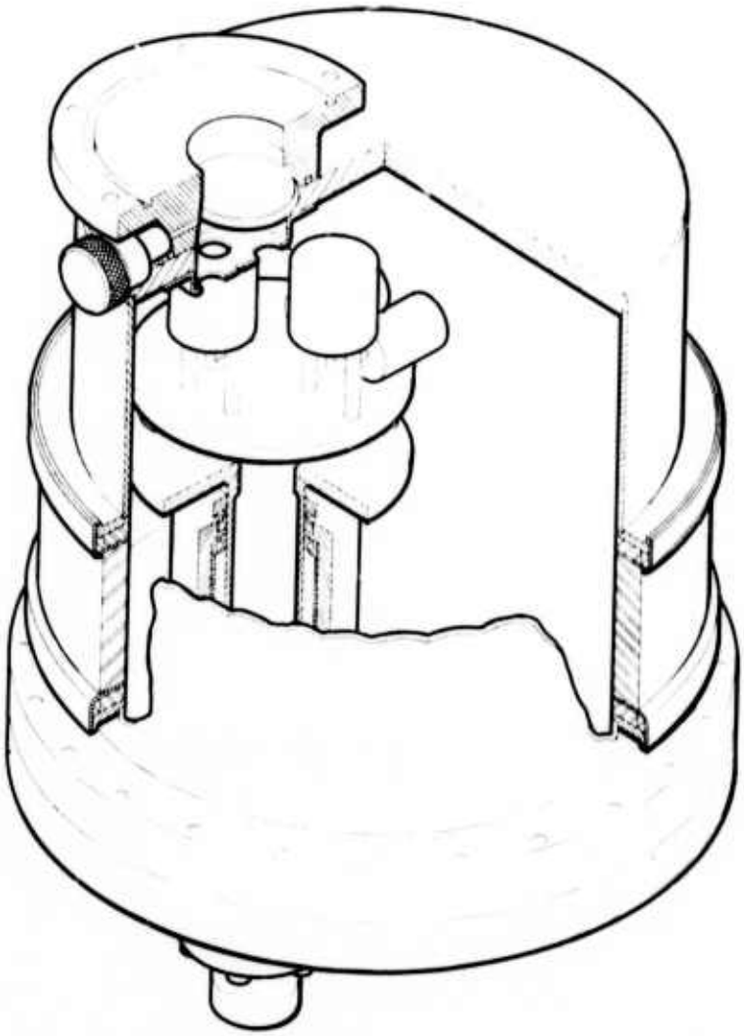

Fig. 27. Isometric view of source chamber showing detail of source positioning mechanism.

by two thin-wall precision bearings which rotate in a bearing housing attached with screws and dowels to the main vacuum interface flange. The rotating shaft is sealed by an O'ring located between the bearings and vacuum enclosure in order to assure proper sealing and placement of the bearings outside the vacuum environment. A collar and belleville flat spring prevent axial motion of the rotating assembly within the housing. Two micrometer stops are provided to allow 90° rotation which is adjustable at each stop by differential screw type micrometers having a range of 0.010 in. each. A two-to-one lever arm arrangement should provide a resolution of 0.0001 in. after initial alignment is accomplished.

The ion sources are supported on an insulated base assembly which is pre-aligned with the desired beam centerlines using conventional precision surface plate and electronic indicator techniques. All mounting interfaces are doweled in place with respect to the locating dowel pins located on the main mounting flange.

A Varian instrumentation electrical feedthrough is provided for wiring of heaters, reservoir valves, and thermocouples as required. This feedthrough is capable of withstanding voltages to 7 kV pin-to-pin before arcing failure occurs.

4. Vacuum Chamber Design

The basic vacuum chamber design is shown in Figs. 27 and 28. This assembly mounts directly to the ion column mounting surface with screws and dowels as specified in previous communication with ARL. A separate vacuum valve is provided to allow roughing of the chamber by existing pumps on the ion column. A liquid nitrogen cold trap is provided to condense cesium and iodine vapors present in the system and a small butterfly valve isolates the chamber from the ion column for source removal and cleaning. An alternative to the panel type cold trap desi which would provide better cleaning capabilities was discussed at the design review held at the end of Phase I of this contract. A large (4 in.) gate valve could be attached to the chamber and a cold trap could be provided which is removable from the

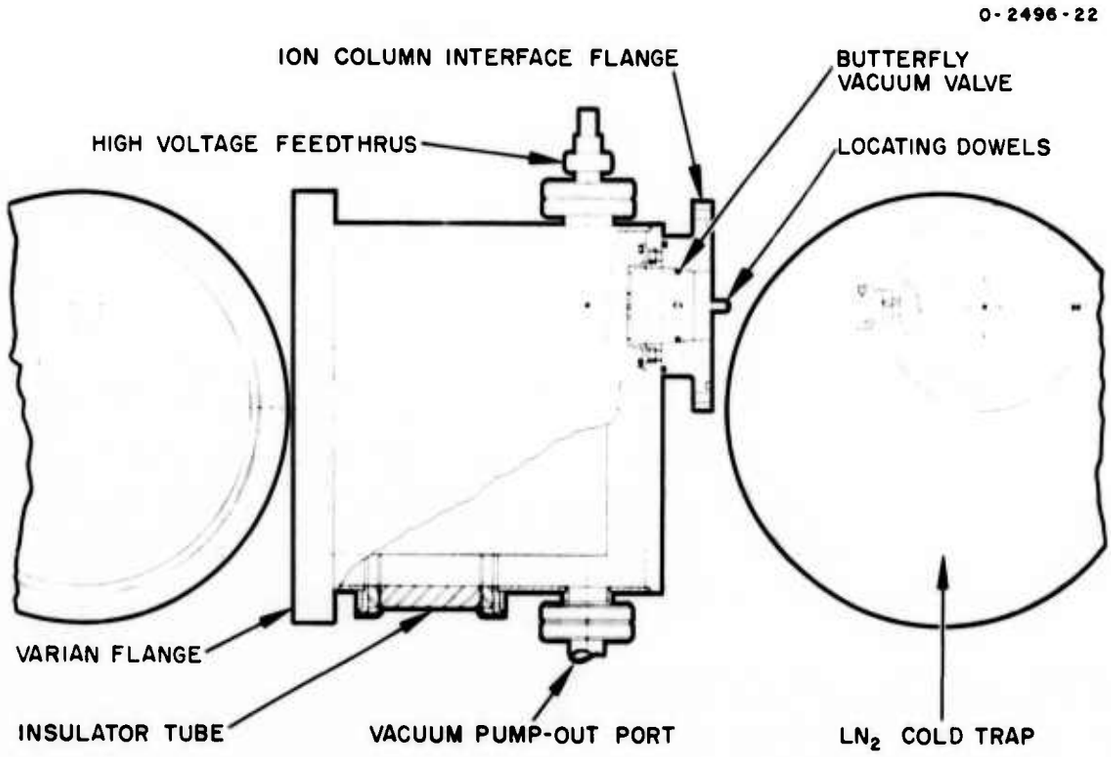

Fig. 28. Layout of ion source vacuum chamber.

system while cold to facilitate easy cleaning of condensed elements while the system is kept under vacuum. This concept requires further discussion to determine if enough room is available, or if this feature is desired in the final design.

The positioning mechanism source mounting flange is isolated from the ion column by a large alumina insulator to provide 20 kV isolation from the ion column. The insulator assembly is welded to the vacuum enclosure by metal flanges which are copper brazed to the insulator tube.

The anode electrodes are electrically terminated through separate high voltage feedthroughs mounted on the vacuum enclosure.

IV. CONCLUSIONS AND SUMMARY

The analytic and experimental studies conducted during Phase I of this program indicate that it is possible to design both cesium and iodine sources to meet the specified brightness requirements of 200 and 100 A/cm^2 sr respectively. No reasons were uncovered as to why these two types of sources cannot operate in the same vacuum environment in such a manner that the ion species available to the AMS can be rapidly changed. Prototype hardware will be developed in Phase II to demonstrate this ability.

REFERENCES

1. Integration Contract with General Electric Vallecitos Laboratory. Contract F33615-72-C-0484, 1972-1973.

2. G.R. Brewer, Ion Propulsion, Gordon and Breach (1970).

3. M. Haine, et al., "Characteristics of the Hot Cathode Electron Microscope Gun," Brit. JAP 3,40 (1952).

4. M.E. Haine, et al., "Resistance Bias Characteristic of the Electron Microscope Gun," Brit. JAP 9, 482 (1958).

5. V. Braucks, OPTIK 15, 242 (1958).

6. A.N. Broers, "Electron and Ion Probes," Fifth International Conference Electron and Ion Beam Science and Technology.